Spring 2021

Temperature Dependence of Electroluminescence and Current-Voltage Characteristics of Arrays of Deep Ultraviolet Algan Micropixel Led

Dhruvinkumar Prakashchandra Patel

TEMPERATURE DEPENDENCE OF ELECTROLUMINESCENCE AND CURRENT-VOLTAGE CHARACTERISTICS OF ARRAYS OF DEEP ULTRAVIOLET AlGaN MICROPIXEL LED

by

Dhruvinkumar Prakashchandra Patel

Bachelor of Engineering
Gujrat Power Engineering and research Institute, 2017

Submitted in Partial Fulfillment of the Requirements

For the Degree of Master of Science in

Electrical Engineering

College of Engineering and Computing

University of South Carolina

2021

Accepted by:

Ahmad Iftikhar, Director of Thesis

Asif Khan, Reader

Tracey L. Weldon, Interim Vice Provost and Dean of the Graduate School

ACKNOWLEDGEMENTS

I would like to acknowledge my advisor Dr Ahmad Iftikhar for guidance, support, and patience through my graduate studies. I would thank Dr Asif Khan for allowing me to do thesis on low temperature study of micro DUV LED. I would like to thank Dr Mikhail Gaevski for guide me through thesis and experiment setup. I would like to thank Dr Chandra to guide me for analyses data and help me for circuit model and simulation.

I would like to thanks to Richard for help me throughout thesis and guide me for experimental setup and guide me for data analysis. I would like to thank my lab mates Samiul, Didar, Kamal, Shahab for their help with lab equipment and experiment setup.

I would like to thanks to my family and relatives for support me. Without the support from my loving parents, I would not have reached so far.

ABSTRACT

III-Nitride based deep ultraviolet (DUV) light emitting diodes are non-toxic light sources that are highly desirable to replace current mercury lamp-based technology for air and water purification, surface and object disinfection, and sterilization. In the present. By freezing out defect related conduction pathways at temperatures less than 50K, the external quantum efficiency (EQE) of an interconnected array of 1,296 AlGaN DUV micropixels is improved by 4 times, underscoring the importance of defect management. Assuming a current injection efficiency (CIE) of 100% and considering that the light extraction efficiency (LEE) is constant with temperature, the 4-fold increase in the EL signal is attributed to the increase of the internal quantum efficiency (IQE). A thorough investigation of the current-voltage (I-V) characteristics revealed two distinct slopes with turn-on voltages of 2.7 V and 4.5 V. The low turn-on voltage path indicates the presence of defects in the bulk material and the higher turn-on voltage path is attributed to the multiple quantum well (MQW) active region. The turn-on voltage of 6.4 V at room temperature is larger than that expected from the active layer band gap of 4.3 eV and increases significantly with decreasing temperature. The contact resistances are likely responsible for the increased turn-on voltage with decreasing temperature. Remarkably, the series resistance of the device in high current regime that determined by highly resistive p-AlGaN layers of the structure, is nearly independent of temperature. This confirms polarization doping mechanism in these layers with reverse graded Al contents.

TABLE OF CONTENTS

LIST OF FIGURES

LIST OF SYMBOLS

τ	Radiative lifetime.
τ_{nr}	Non radiative lifetime.
η_0	External quantum efficiency.
η_{inj}	Injection efficiency
η_r	Radiative efficiency.
η_{opt}	optical efficiency

LIST OF ABBREVIATIONS

AlN.....Aluminum nitride

AlGaN.....Aluminum Gallium nitride

DUV..... Deep ultra-violet

EBL.....Electron blocking layer

EL..... Electroluminescence

EQE.....External quantum efficiency

GaN.....Gallium nitride

InGaN.....Indium-Gallium nitride

IQE .....Internal quantum efficiency

LD .....Laser diode

LED.....Light emitting diode

MBE.....Molecular beam epitaxy

MOCVD..... Metal organic chemical deposition

MQW .....Multiple- Quantum well

UV.....Ultra-violet

CHAPTER 1

INTRODUCTION

Group III nitrides have unique physical, electrical, and optical properties that guarantee demand for them in modern optoelectronic and microelectronics under harsh environments. Group III nitrides have wide band gape, high thermal stability conductivity, high breakdown voltage and high radiation hardness [1]–[3]. Due to these properties III nitrides materials are widely used for developing high power ultra-violate (UV) and visible, light emitting diode (LEDs), laser diodes (LDs), and microwave transistors. Shuji Nakamura first demonstrated high brightness blue LED using III-nitride materials, Indium-Gallium nitride (InGaN) and Gallium nitride (GaN), which lead to the development of GaN based optoelectronics [4]. The high brightness, highly efficient blue and green LED developed by Nichia on sapphire substrate using InGaN/GaN, and Aluminum Gallium Nittride (AlGaN) double heterostructure LED [5], [6]. The further research on III-nitrides led the researcher to th development of short wavelength UV LED.

III-nitride based (AlGaN) research on UV-LEDs for wavelengths shorter than 360 nm was started between 1996 and 1999 by several research groups worldwide [7]–[9]. DARPA initiated the program “Semiconductor Ultraviolet Optical Sources (SUVOS)” in the US to spur the research in the field of deep-UV light sources. The group at the University of South Carolina (USC) reported the first 250nm and 280 nm AlGaN-based UV LEDs between 2002 and 2006 [10]–[12]. Other active groups in this area of research

were at Texas Tech University (TTU)[13], [14] and Kansas State University [15]. In Japan groups at RIKEN (Japan's largest comprehensive research institution), Majio University, and Nippon Telegraph and Telephone (NTT) laboratory perused this research aggressively at the same time. A group at NTT reported the shortest wavelength (210 nm) LED using an AlN emitting layer in 2006[16]. At RIKEN AlGaN-based research on DUV-LEDs started in 1997. They have developed high-efficiency UV LEDs using indium incorporation into AlGaN on different substrates[9], [17]–[19]. In Germany, III-nitride based UV-LED research was started at UT Berlin in 2005 by M. Kneissl from Palo Alto Research Center[20]. They developed III-nitride based UV-LEDs in 2006 and 2007 using hydride vapor phase epitaxy to grow AlGaN and AlN templates for LED structures. Latter other research institutions in S. Korea at Pohang University and Samsung [21], [22] and China at Peking University started to work on this technology[23], [24]

Figure 1.1 shows the status of the external quantum efficiency (EQE) of III-nitride based UV-LEDs emitting below 300 nm wavelength covering UV-C, which starts from 280 nm wavelength, as measured at room temperature[25]. The data points are the subset of the data given in reference[25]. The research focus, seen by the cluster of points around 280 nm, to develop high efficiency 280 nm-band AlGaN DUV LEDs is driven by its application for sterilization proposes, which has promising market potential. EQE is the product of IQE, IE, and LEE. It is seen that the EQE of most of the LEDs emitting at and below 300 nm wavelength is in single digit, in comparison to UV-LEDs emitting around 363 nm is between 46% to 74%[26].

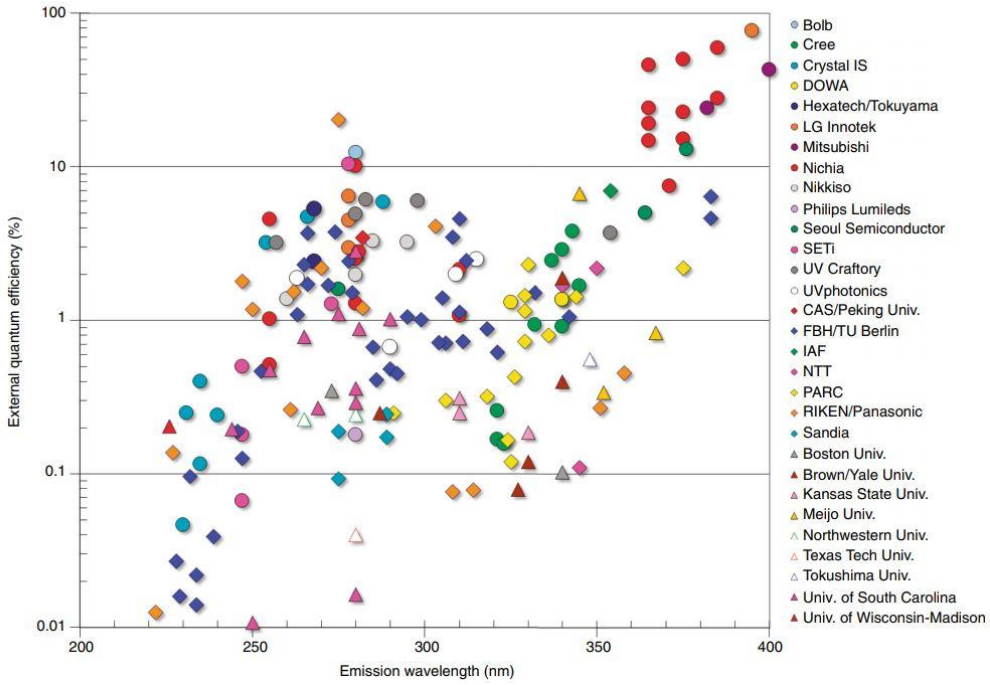

Figure 1.1 A brief survey of EQE vs wavelength for UV-LEDs Emitting < 300nm [complete data set is given in reference [25]].

The improvement of the EQE for LEDs emitting around 280 nm started with the low threading dislocation density AlN templates[17], [27], [28] and n-AlGaN layers[29]. Low dislocation density AlN layers led to high IQE of (>60% %) for AlGaN and quaternary In AlGaN QWs in the DUV region[30], [31]. Further development of the electron blocking layer (EBL), that prevent the electron spillover into p-AlGaN/p-GaN, resulted in an increase in the injection efficiency[32]–[35]. To further increase EQE, efforts were made to improve LEE in UV-LEDs by transparent LED layer, high reflective p-contacts, backside surface patterning, device shaping and growth on patterned sapphire substrates[19], [36]–[40]. These developments led to a recent breakthrough performance of 20 % EQE by RIKEN in collaboration with Panasonic[41]. The problem is the driving voltage for this LED is very high (16 V), which will result in severe Joule heating, thus not a practical solution.

The contributions of the companies in the development of UV-LEDs emitting in the range of 260 nm to 300 nm cannot be neglected. Here, Sensor Electronic Technology Inc. (SETi) commercially produced UV-LEDs having wavelength range from 240 to 300 nm and for 278 nm UV-LED achieved a maximum EQE of 11% on sapphire substrate[42]–[44]. Crystal IS and Tokuyama reported 5-7 % EQE for deep UV-LEDs on single crystal AlN layers produced by sublimation[41], [45] and hydride vapor phase epitaxy (HVPE)[46], [47] respectively. Similarly, high-efficiency UV-LEDs were produced by UV Craftory, Nitek, and Nichia[31], [48], [49]. UV Craftory has reported UV-LEDs with EQE of 14.3 % with very low current injection.

UV-LEDs are solid state devices that produces light when electrical current can flow from the positive (p-type) side of circuit to negative (n-type) side of the LEDs. It has been attracting significant attention as a new UV source, it can replace conventional mercury lamps in the water disinfection applications [50], [51]. UV LEDs emit a narrow band of wavelengths of light from the junction and their wavelengths span the spectrum ranges from 200 nm to 400 nm as shown above in Figure 1.2[52]. Based on emitted wavelength UV-LEDs are divided into near-ultraviolet light-emitting diodes (NUV-LEDs), with emission wavelength ranges approximately from 300–400 nm, and deep-ultraviolet LEDs (DUV-LEDs), with emission wavelength ranges approximately from 200 nm–300 nm. UV-LEDs are promising candidates for various applications like disinfection & sterilization, analytic use (forensic), air purification, water purification, resin curing, biochemistry sensing which represent in Figure 1.3 [52]. UV LEDs are not only mercury free, but also can have a higher energy efficiency, a longer lifetime, more constant light intensity, that is easier to control than their counterparts.

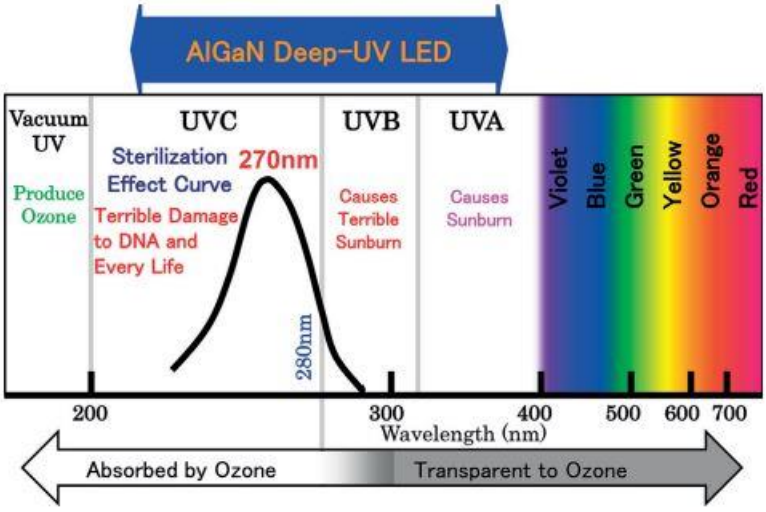

Figure 1.2 UV LED wavelength spectrum [52].

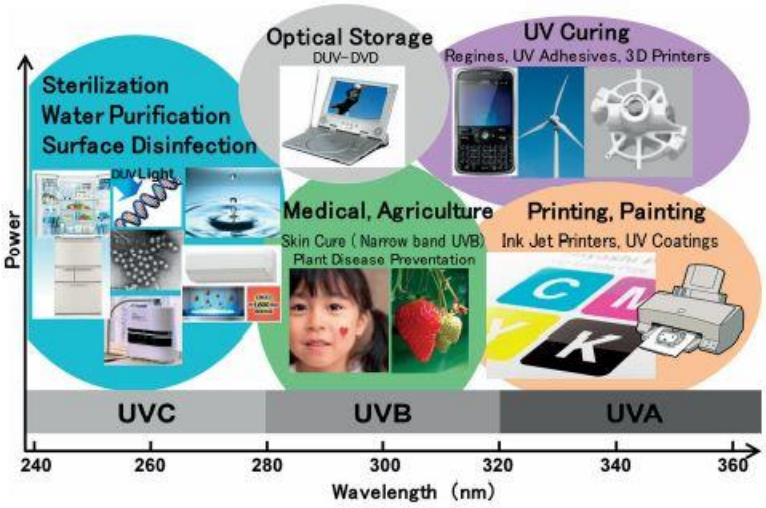

Figure 1.3 Application of DUV light emitting diode [52].

1.1 Fundamentals of Light emitting diodes

To understand light emission from LEDs, we need to understand their physical properties. LED are simply p-n junction diodes that convert electrical power to infrared visible or ultraviolet light through spontaneous recombination recombination[53]. The emitted wavelength is determined by the bandgap of the semiconductor's material used. LEDs only work in forward bias conditions, as shown in figure 1.4, electrons are injected

from n- type into p- type and hole from p type to n type layer. In a diode, under forward bias current easily flow from p-side to n-side but it does not flow reverse biased condition. For Group III nitrides LED, the emitting region consist of $Al_xGa_{1-x}N$ (where x is the Al percentage), called active region is sandwiched between anode (p type) and cathode (n type) $Al_xGa_{1-x}N$. This $Al_xGa_{1-x}N$ have single or multi-quantum well region to increase the recombination probability.

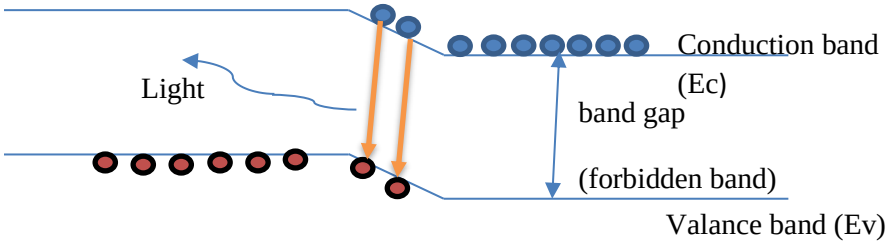

Figure 1.4 Band diagram of p-n junction.

1.1.1 Radiative and non-radiative recombination

There are mainly two types of recombination mechanisms in semiconductor, radiative and non-radiative recombination. Radiative recombination is generally band to band recombination. In radiative recombination, a photon with energy equal to the bandgap energy of the semiconductor is emitted, which is represented in Figure 1.5. In non-radiative recombination, the electron energy is converted to vibrational energy like phonon, which produces heat which is illustrated in Figure 1.5. The Recombination rate is proportional to both electron and hole concentration.

$R \propto n \times p = B_r \times n \times p$

where R is the recombination rate per unit volume and B_r is coefficient of band-to-band recombination and n and p are the electron and hole densities.

$R = B_r \times (n_{n,0} + \nabla n) \times (p_{n,0} + \nabla p)$

Where $n_{n,0}$ and $p_{n,0}$ are densities of electron and holes at equilibrium in n and p type materials and ∇n and ∇p are electron and holes excess carrier densities, respectively. The spontaneous recombination rate for the excess carrier is given by

$R_{sp}^{ex} = \frac{\nabla n}{\tau}$ where τ is a radiative lifetime

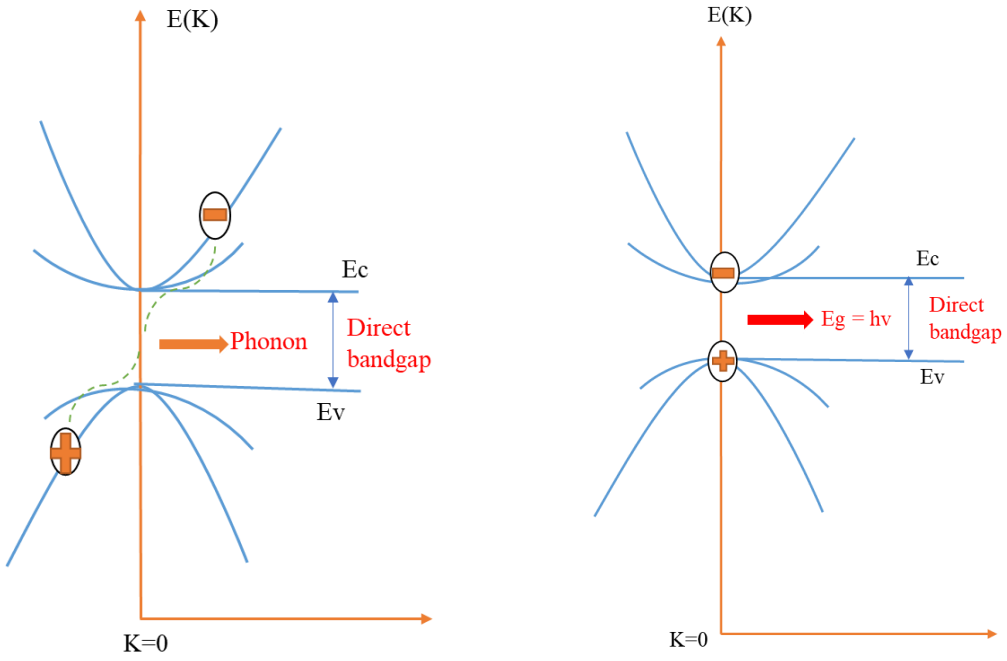

(a) (b)

Figure 1.5 (a) Non-Radiative combination, and (b) Radiative recombination.

1.1.2 External quantum efficiency (η_0)

External quantum efficiency (EQE) defined as the number of photons generated by the applied current, so External quantum efficiency (EQE) is defined as total optical power divides applied electrical power. In simple terms, LED efficiency is defined as how much light is generated for injected current. We can write:

η_0= overall External quantum efficiency = $\frac{Number\ of\ photon}{Number\ of\ electron}$

The other way to define the EQE is

$\eta_{0ext} = \eta_{inj} \times \eta_r \times \eta_{opt}$

where,

η_{inj} = Injection efficiency

η_r = radiative efficiency

η_{opt}= optical efficiency

Injection efficiency

The injection efficiency is defined as the ratio of the number of photons emitted from the active region per second to the number of electrons injected into LED per second [2].

η_{inj} = Injection efficiency = $\frac{number\ of\ photon\ emiteed\ from\ active\ region\ per\ second}{number\ of\ electron\ injected\ into\ LED\ per\ second} = \frac{Pint/(hv)}{I/e}$

Where P_{int} is optical power emitted from active region and I is Injection current and e is the charge of the electron.

Injection efficiency in term of materials properties defined as below,

$\eta_{inj} = \frac{nDnLn}{nDnLn + pDpLp}$

Dn and Dp are diffusion coefficients of the electron and hole and L_p and L_n are diffusion lengths of minority carriers and n and p are net electron and hole concentration.

Radiative Efficiency

Radiative efficiency is defined as the ratio of the total number of electron-hole pairs that combine radiative to the total number of electron- hole pairs recombine in the active region. The radiative efficiency also known as internal quantum efficiency (IQE). The IQE is defined as the ratio of the radiative recombination to the total recombination[2].

η_{r} = radiative efficiency = $\frac{\tau}{\tau r} = \frac{1}{1+\tau r/\tau nr}$

where,

τ_r = radiative lifetime

τ_{nr} = non radiative lifetime

Optical Efficiency

The amount of light that come out from LED determine optical efficiency which is also named as extraction efficiency (IE) of LED called optical efficiency. Theoretically some LEDs have unity extraction efficiency; however, in practic not all power emitted from the active region is emitted in free space. Some of the photons may never leave semiconductor LED die; this is due to some losses in the device. For example, some light reabsorbed in the substrate of LED and other materials of the device like, substrate contact layers and contacts. There are several factors that affect the extraction efficiency like the absorption coefficient of semiconductors, layer structure, and refractive index of the semiconductor layer. The extraction efficiency is defined as the ratio of the number of photons emitted into free space to the number of photons emitted from active region[2].

$\eta_{extraction} = T_{SE} \times T_{EA} \times \eta_{esc}$

where,

T_{SE} is Reflection and transmission through the semiconductor epoxy interface, T_{EA} is transmission through the epoxy-air interface and η_{esc} is efficiency related to light extraction through the escape cone.

$T_{SE} = \frac{4\eta s \eta e}{(\eta s+\eta)2}$

$T_{EA} = \frac{4\eta e}{(\eta e+1)2}$

$\eta_{esc} = \frac{1-\sqrt{1-(\eta e/\eta s)2}}{2}$

So total extraction efficiency = = $\frac{1-\sqrt{1-(\eta e/\eta s)2}}{2} \times \frac{4\eta e}{(\eta e+1)2} \times \frac{4\eta s\eta e}{(\eta s+\eta)2}$

where,

ηs = Refractive index and ηe = Epoxy encapsulation refractive index

1.1.3 Hetero structure/ Multi- Quantum well

There are two general possibilities to increase internal quantum efficiency. The first possibility is to increase radiative recombination and the second is to decrease the non- radiative recombination. The radiative rate increases with free carrier concentration; therefore, it is important that recombination in which region of LED occurs has a high carrier concentration, therefore, incorporating the heterostructures is the way to increase carrier concentration[2]. We can make heterostructures by combining wide bandgap semiconductors with narrow bandgap semiconductors. By proper combination we can achieve the highly efficient heterostructure LED. Figure 1.6a and Figure 1.6b, we illustrate homojunction and heterojunction LED under forward bias condition, respectively.

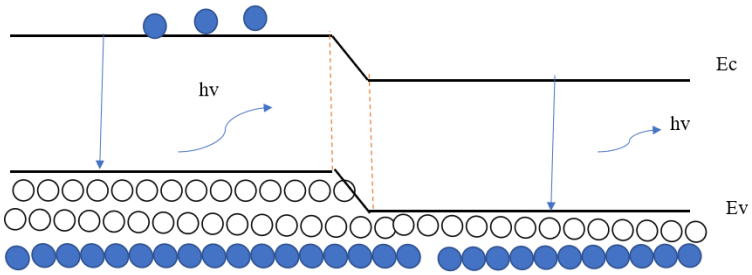

(a)

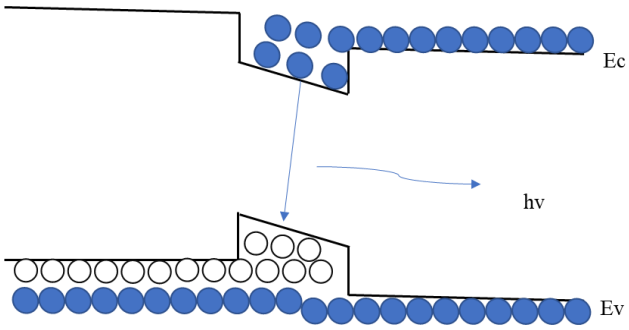

(b)

Figure 1.6 (a) Homojunction, (b) Heterojunction under forward bias.

1.2 Material selection for UV LED

Group III nitrides have wide band gape, high thermal conductivity, high breakdown voltage and thermal stability. Due to these properties III nitrides materials widely used for developing high power ultraviolet (UV), blue and green light emitting diode. Depending on Al content, band gap of AlGaN can be change on 3.4eV to 6 eV. The band gap of AlN is 6.2 eV, GaN is 3.4 eV and InN is 1.9 eV is shown in the figure 1.7[1]. Figure 1.7 represents bandgap energy versus bond length for III- nitride materials. III-Nitride materials have high thermal stability and good conductivity. The direct bandgap of GaN and its alloys enable these materials to be used for optical and electrical applications. At 300 K (room temperature), GaN direct bandgap is 3.44 eV which near to Ultra violate (UV) region of the optical spectrum [54]. The spectrum of $Al_xGa_{1-x}N$ alloys is near to DUV region so it is the perfect materials for DUV LED.

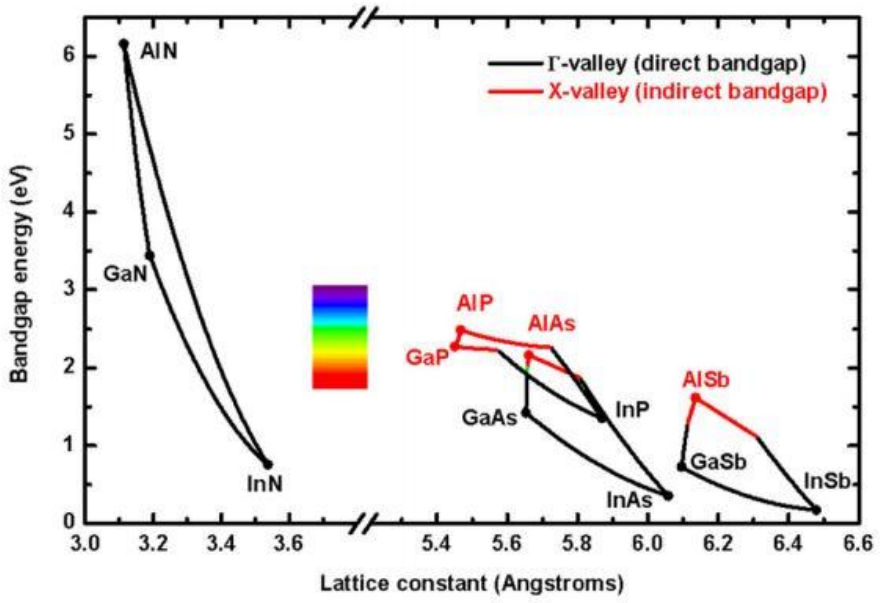

Figure 1.7 Band gap Energy vs lattice constant III- nitrides at 300 K[1].

1.3 Motivation to study Micro- DUV LED at Low temperature.

III-Nitride optoelectronic devices have been replacing technology at the amazing rate. AlGaN based deep ultraviolet LEDs are available for commercial application. Milliwatt- powers of AlGaN DUV LEDs have been reported by several group with improved performance[10], [55], [56]. Besides, the external quantum efficiency and wall plug efficiency of AlGaN LEDs are less compared to visible LED [57]. This is due to lower extraction efficiency and self-heating of LED (thermal issue) which can be reduce but not eliminated by flip-chip LEDs[58]. In a Chitins et al. report on self- heating effect in ultraviolet light emitting diode, they applied 50mA DC pump current and measured in increased study state temperature of about 700^0 C which reduced output power of LEDs[58]. Hao G et al. illustrate current crowding in 280nm DUV AlGaN based flip-chip LEDs, they determine that the current spreading length is small in DUV LEDs which cause current crowding and self-heating which is responsible for efficiency drop

and power saturation[59]. Due to efficiency drop, power saturation, and reduce lifetime, we focus on the study of AlGaN based Micro- DUV LEDs [60].

Recently,Floyd R et al. reported AlGaN based DUV micro-LEDs[60]. They presented different pixels (5um to 15 um) sizes of AlGaN multi-quantum well based micropixel DUV LEDs. They design a LED in such a way to avoid current crowding and high extraction to get high brightness and high power DUV emission. We have not seen any report for the temperature dependence of electroluminescence (EL) and current-voltage characteristic of AlGaN based DUV micro-LED. Zang J et al. illustrated low temperature electroluminescence quenching of AlGaN deep- ultraviolet light-emitting diodes [61]. They study three different AlGaN DUV LED, in which two LED do not have Electron blocking layer (EBL) and one have EBL where they observed EL quenching in AlGaN DUV LEDs which do not have EBL. A Chitnis et al. studied the electrical and optical properties of 285 nm AlGaN single-quantum-well DUV LED at a wide temperature range of 10 to 300 K; they found that EL intensity increases with a decrease in temperature[62]. Several groups reported temperature dependent studies of electroluminescence and electrical properties of LEDs [61]–[64]. To date no study of temperature dependence of electroluminescence (EL) and current-voltage characteristic for AlGaN based DUV micro-LED have not been reported.

In this thesis we study the electroluminescence (EL) and current-voltage characteristic of AlGaN based DUV micro- DUV LED at low temperatures. We expected that electroluminescence (EL) increases or decrease with temperature. Zang J illustrates low-temperature electroluminescence quenching of AlGaN deep- ultraviolet light-emitting diodes[61] while Chitnis find an increase in electroluminescence (EL) in single

quantum well based light emitting diode [62]. If electroluminescence (EL) increases with a decrease in temperature, we expected that current injection efficiency increases so overall efficiency of LEDs increase at low temperature. Micro DUV LEDs have high Al-content $Al_xGa_{1-x}N$ allow are suitable to the formation of threading dislocation, defect like dislocation freeze out at the low temperature and give high electroluminescence (EL) therefore we can use Micro- DUV LED for application under low temperature condition. We are also studying the electroluminescence (EL) properties of DUV LEDs at liquid helium temperature and liquid nitrogen temperature and compare them with Micro-pixeled DUV-LED to see what advantage's different structure present. It is known that defects start to freeze out at liquid helium temperature and result in high electroluminescence (EL), the comparison for the different LED structure gives aa lot of information about the current transport mechanism at low temperature. V-I characteristic of DUV LEDs with temperature enables us to isolate different transport channels.

1.4 Synopsis of this Dissertation

This dissertation presents a study of AlGaN based micro-pixel DUV-LED at low temperatures and its comparison with conventional DUV-LED for the first time.

Chapter 1 present the overview of III nitrides UV LEDs and their application in various fields. The fundamental physics of LED also discuss in this chapter. We also describe materials selection for DUV LEDs and the motivation of micro-LEDs at low temperature.

Chapter 2 focuses on the practical aspects that include the growth of device using Metal Organic Chemical Vapor Deposition (MOCVD) technique and device fabrication and packaging. We also describe the wire bonding of micro-LEDs in the same chapter

Chapter 3 presents the experimental procedure to obtain the data for this dissertation. We discuss the overview of cryostat in this chapter. Overview of spectrometer and semiconductor parameter analyzer also addressed in this chapter. We also describe the Device testing conditions and consideration for low temperature measurement of DUV LEDs

Chapter 4 describe electroluminescence (EL) and current- voltage characteristic of AlGaN based DUV LEDs.

Chapter 5, In this chapter we discuss about dissertation conclusion and recommendation for future work in the field of low-temperature study of DUV-LEDs of different structural configuration.

CHAPTER 2

STRUCTURE AND FABRICATION OF DUV LEDS

In chapter 1, we briefly discuss the fundamental of DUV LED and application of DUV LEDs in various fields. We also discussed our motivation to study Micro- DUV LED at low temperature. In chapter 2, first, I will describe the growth of devices (UV-LEDs) using Metal Organic Chemical Vapor Deposition (MOCVD) technique. After that I will discuss the processing of the DUV LEDs.

2.1. Growth Details

During the last two decades researchers used different techniques for III -nitrides growth like Liquid phase Epitaxy (LPE), Molecular Beam Epitaxy (MBE), Vapor Phase Epitaxy (VPE) and Metal Organic Chemical Vapor Deposition (MOCVD). High quality epitaxial layer can be grown by MBE and MOVCD [3]. But Molecular Beam Epitaxy (MBE) is expensive system that required ultrahigh vacuum for growth and highly complex system. Generally, researcher use MOCVD for growth of III nitride material which is very flexible, easy to control, good growth uniformly and produce sharp interface. High quality quantum structures like multi-quantum wells (MQWs), double heterostructure can easily be grown by MOCVD which is widely used for electronic and phonics devices. The epilayers of our LED structure were produced by MOCVD.

A homemade MOCVD system was used to growth devices used for this dissertation. Figure 2.1 represent the schematic diagram of MOCVD system [65]. MOCVD system a standard inductive rf heated system with cold vertical reactor

chamber. The MOCVD system is capable of depositing very thin layer of atoms of III-nitride onto different substrate, in our case sapphire wafers. Semiconductor wafers are usually made from sapphire or silicon which are cheaper and easily available; here the devises are grown on sapphire wafers. There are different sources of materials use for the growth process. Trimethylgallium for Gallium (Ga), trimethylaluminum for aluminum (Al)[66] and ammonia is used for nitrogen as the sources. Silane used for silicon (Si) n type dopant and biscyclopentadienly magnesium (Cp_2MG) Mg is used for p type doping[66]. The MOCVD vertical chamber reactor and rf type high inductive heating which requires a good quality quartz chamber which is nonconductive and transplant[67]. The reactor chamber able to sustain up to 1150 ^{0}C. The precursors are inserted through various lines in the reactor the through showerhead which are designed a such a way to inject different precursors and distribute them uniformly over the substrate on heated susceptor. The showerhead is made from stainless steel and the susceptor is made from silicon carbide. During growth, Susceptor is rotating which provide uniform distribution on wafer. The different sizes of gas tubes for MOCVD system are made from stainless steel to reduce the impurities. For failure or replacement, automatic or manual value are used for isolation of gas flow equipment. In the MOCVD system, nitrogen (N_2) and hydrogen (H_2) are generally used for carrier gases and mass flow controllers control their flows. The exhaust of MOCVD system after vacuum pump is made from polyvinyl chloride pipes.

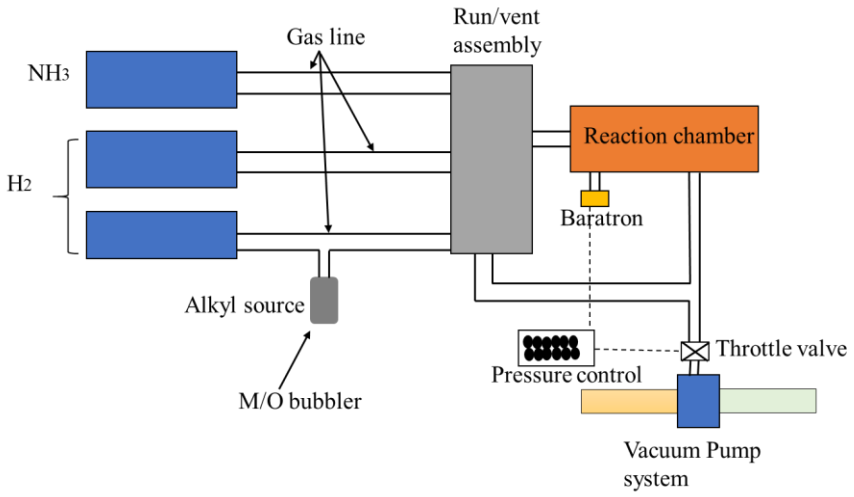

Figure 2.1 Schematic diagram of MOCVD system.

LED structure growth on sapphire substrate starts with the aluminum nitride (AlN) nucleation layer, this layer followed by 3 μm thick thermally conductive AlN, which acts as the templets for further AlGaN layer, grown by the MOCVD system [68], [69]. The thick AlN layer improve overall crystal quality and reduce the number of dislocations in subsequent layers required for device structure. The device structure and epilayer details (not to the scale) are represented in Figure 2.2[60]. The AlN layer is followed by 1.5 μm n- $Al_{0.65}Ga_{0.35}N$. We grow 4 pairs of multiple quantum wells (MQWs) which increase the carrier capture cross-section for the active region [12]. Mg-doped p- $Al_{0.7}Ga_{0.3}N$ electron blocking layer (EBL) was grown after MQWs active layers, decrease the electron injection into the p-GaN/AlGaN layer. This layer is followed by graded p-AlGaN and p-GaN contact layers. The complete details of the growth can be found in reference [55], [60], [70], [71].

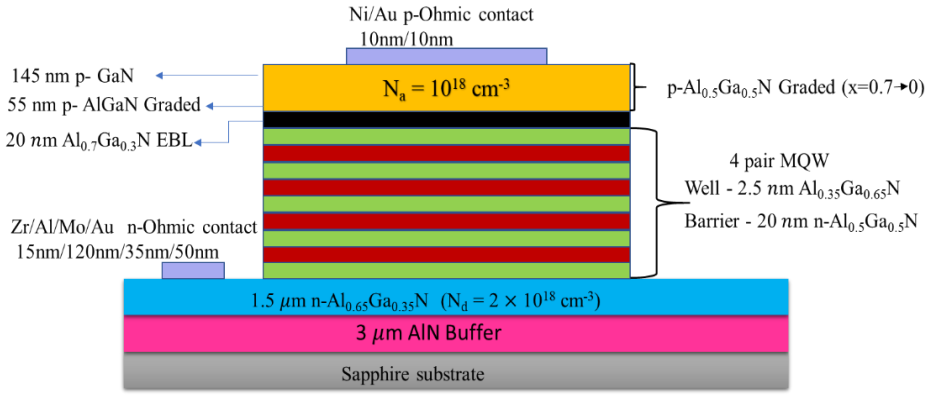

Figure 2.2. Layer structure of UV-LED showing the thickness and composition of each layer.

2.2 Device fabrication

Figure 2.3 represent two different structure of LED, Figure 2.3a represent vertical conduction [12], [71] and Figure 2.3b lateral conduction[60]. Here black arrows the show current flow in the LED structures.

For vertical conduction device, A mesa type square geometry device was fabricated. A reactive ion-etching process was used for bottom n AlGaN layer. The n-contact metal Ti/Au/Ti/Al was deposited at 950 ^{o}C for 1 minute in forming gas[12]. The p-contact Ni/Au was annealed at 500 ^{o}C for 2 minutes in the oxygen environment. For lateral conduction device, first Cl_2/Ar chemistry inductive coupled plasma reactive ion etching (ICP_RIE) is used to define the micropixels and access to the n contact. The nitrogen environment was used at 750 ^{o}C to activate Mg-dopant. The n contact metal stack Zr (150 Å)/ Al (1200 Å)/ Mo (350 Å)/ Au (500 Å) was deposited via electron beam (e-beam) deposition system and annealed at 950 ^{o}C for 3 minutes in forming gas by rapid thermal annealing [60]. The p-contact Ni/Au were deposited by e-beam deposition and annealed at 500 ^{o}C for 5 minutes on hot plate in oxygen environment.

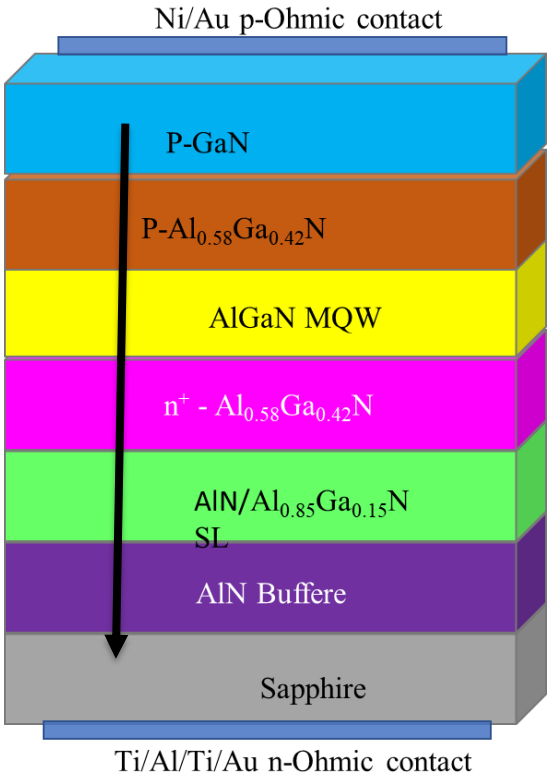

(a)

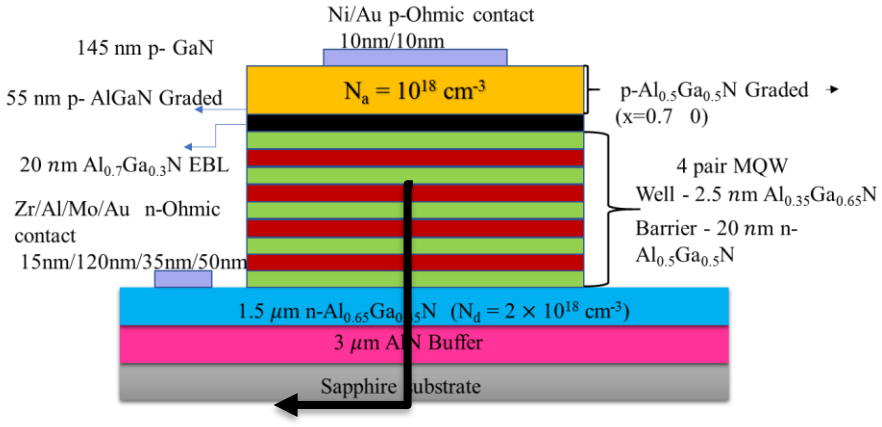

(b)

Figure 2.3 Different LED strcture, a) Vertical cnduction, b) Lateral conduction.

2.3 Packaging

Silicon carbide and Gallium nitride are widely use for substrate for semiconductor device due to high thermal conductivity but both are highely aborbing ultraviolate

wavelength region and are expensive. So, researchers generally prefer to use sapphire substrate due to high lighet extraction efficiency and cheap. However Sapphire has poor electrical and thermal conductivity compare to Silicon or GaN results in at higher operating voltage LEDs and large self heating. That reduces the efficiency of UV-LED. The flipchip method is used to mount the UV-LEDs to reduced the self-heating.

There are different type of flip-chip bonder used in the industry like Au/sn solder attachment and gold (Au) to Gold bump (Au). Earlier our group use Au/sn solder attachement process [58], [70]. Here we use Gold-to-Gold bump bonding that is carried out using a semi-automatic flip-chip bonder shown in Figure2.4. We flip LED dye onto aluminum nitride or silicon carbide sub-mount. The Different headers can be used depending on the application requirement. Generally TO-39 and TO-66 headers are used for DUV LEDs. Figure 2.5a represent a flip-chip device and 2.5b show packaged device. The thermal conduction can be further improved by external heat sinks which may be used with the combination of thermal paste. Shatalov et al. study thermal analysis of flip-chip packaged UV LED, they analyzed that 82% heat energy flow through flip-chip bond[72]. We can improve perfomance of LED's perfomance using flip chip, and minimize the self-heating problem.

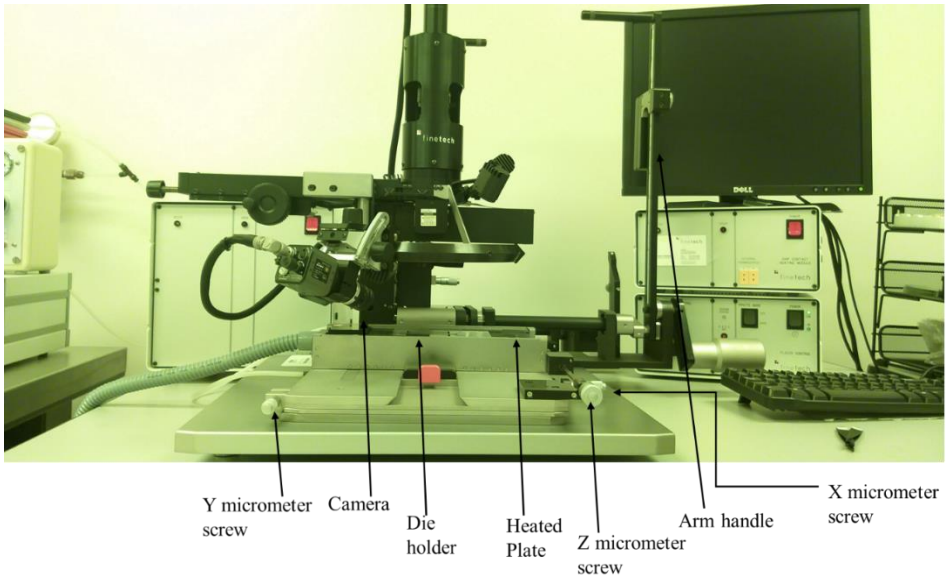

Figure 2.4 Flip-chip bonder.

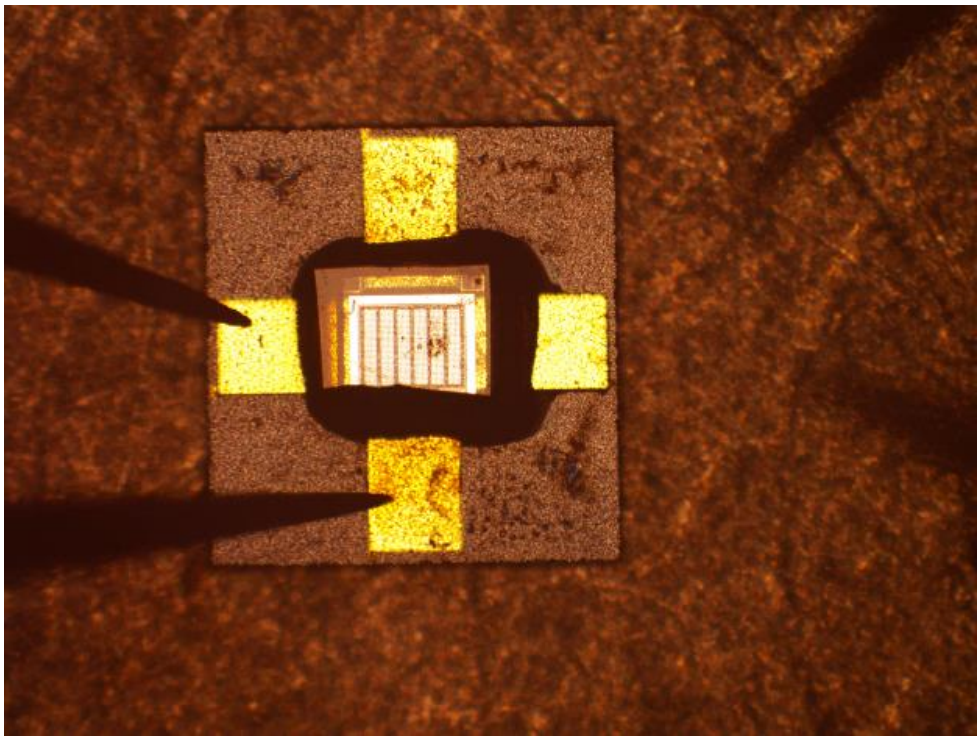

(a)

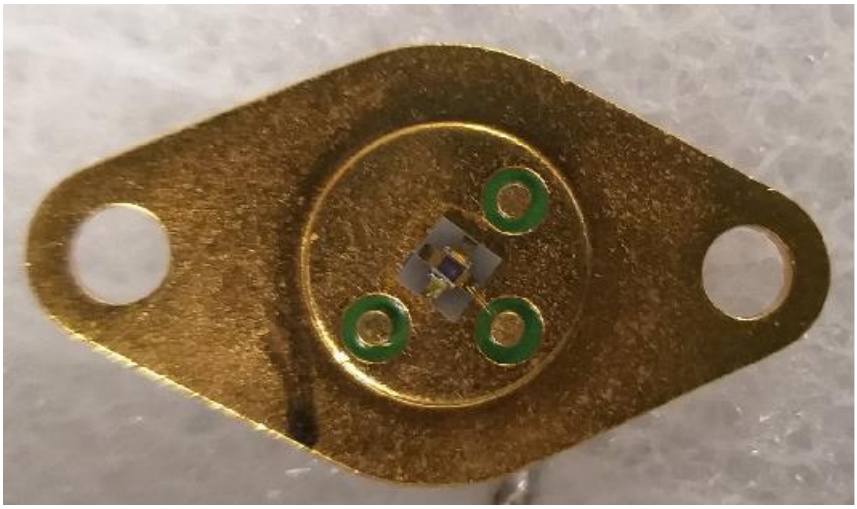

(b)

Figure 2.5 Flip-chip and packaging device, (a) Flip-chip device, (b) Packaging device.

2.4 Wire Bonding

A semi-automatic West bond wire bonder can be used for wedge-to-wedge bonding or Ball-to-wedge bonding. But we used the Ball- wedge bonder for wire bonding. The Semi- automatic thermo sonic bonder applied sufficient thermal and mechanical energy to the gold ball formed at the end of the bond tool.

The base model 747677E use for Ball-to-wedge bonding. The 0.001inch Gold wire use for wire bonding. First, the gold wire pass through clamp and inserted in a Capillary tube for bonding. The diameter of the capillary is 15 inches. Figure 2.6 represent the wire bonder head assembly. The packaging LED sample is attached to hotplate with clam screws. Turning on the hotplate switch to allow the sample to warm up to 140^{o} C in few minutes. To make the first bond, we need to set ultrasonic power and time around 325 and 20ns. To make a second bond, we need to set ultrasonic power and time around 330 and 30ns. For the first bond we use low force and for the second bond

we use high force. The dynamometer uses to measure force. We also need to set high force 30 grams and low force is 21 grams.

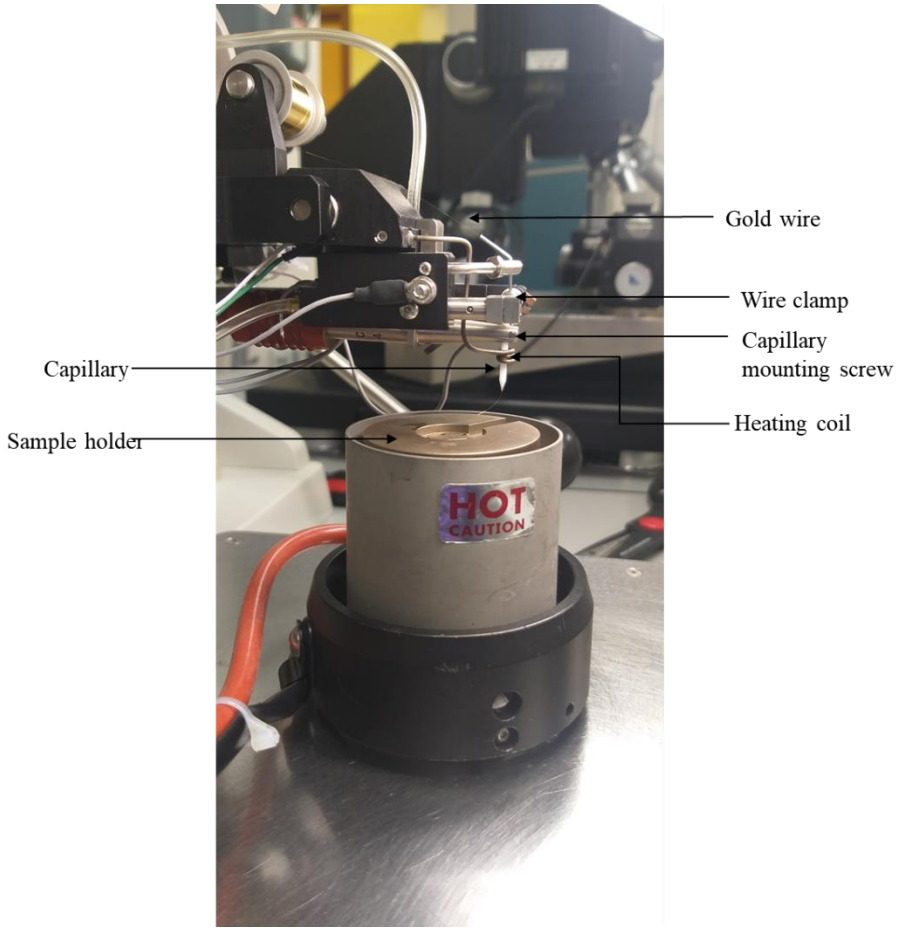

Figure 2.6 The wire bonder head assembly.

The process of gold ball bonding formation is the same as wire bonding on IC die. The gold wire which passes through the capillary tube is an electrical discharge to form a gold ball, that bonded to gold pads on LEDs by thermo-compression and ultrasonic energy. Then we need to move the wire bonder manipulator arm in an upward direction and make a second bond on the AlN sub-mount. The capillary tube clamping the wire is withdrawn and the wire is cut. We can feed the extra wire through a thread switch. Figure

2.7 represent gold and wedge bonding, Figure 2.7a, we show the gold bump on LED pads and Figure 2.7b we indicate wedge bond on AlN sub mount.

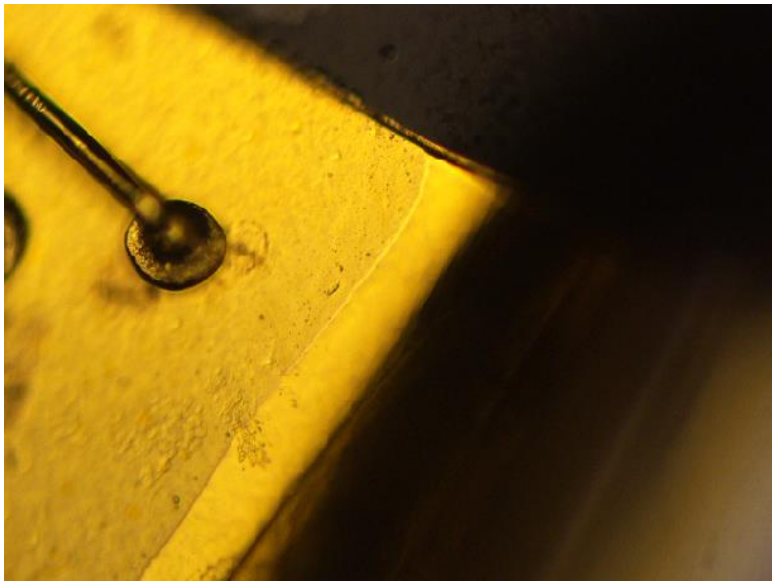

(a)

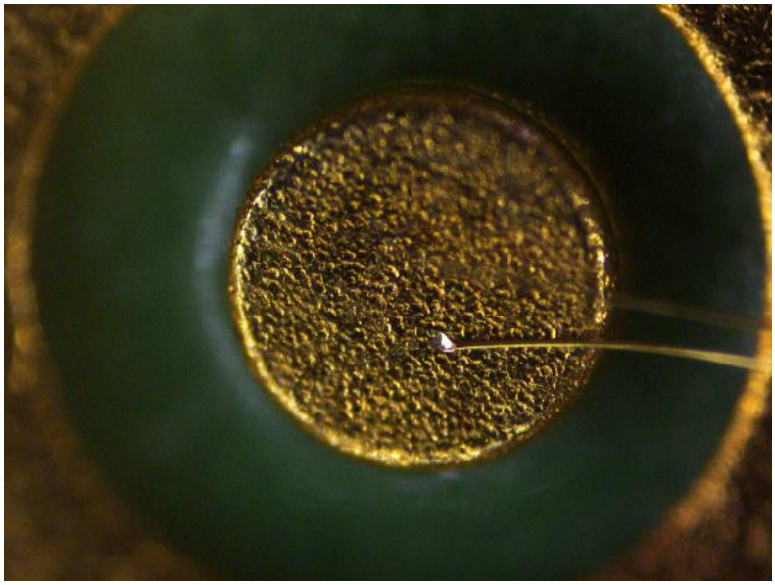

(b)

Figure 2.7 Ball to wedge bonding, (a) Gold ball (bump) bonding, (b) Wedge bonding.

CHAPTER 3

EXPERIMENTAL PROCEDURE

In chapter 2, we briefly discuss MOCVD process, layer structure, and packaging process of DUV LEDs. In this chapter we will describe the experimental procedure of low temperature study of LEDs. This description includes an overview of the cryostat, parameter analyzer, and spectrometer. This followed by the description device testing condition and consideration

3.1 Closed cycle cryostat setup

This section illustrates a cryostat setup for studying the spectral and optical properties of LEDs at low temperatures. Typically, a Closed Cycle Cryostat is used to attain the low temperature at a very small region inside the vacuum environment to avoid condensation. The electrical feedthroughs and optical windows in cryostat are used for measurement like electrical and optical properties of the devices. Figure 3.1 represents a schematic diagram of closed-cycle cryostat setup. The major components of the closed cycle cryostat are compressor, cold head, vacuum shroud, radiation shield, optical windows, temperature controller and vacuum system. The expander portion of the cryostat is commonly referred to cold head, where the Gifford-McMahon refrigeration cycle takes place. The cold head is connected to a compressor by two gas lines and an electrical power cable. One gas line supplies high- pressure helium gas to the cold head where it expands and cause cooling in the expander and the second gas line returns low pressure helium gas from the expander to the compressor. The compressor provides the

flow to the low-pressure and high-pressure helium gas from and to the expander to attain desired refrigeration capacity. The temperature controller is also connected to an expander to control the temperature.

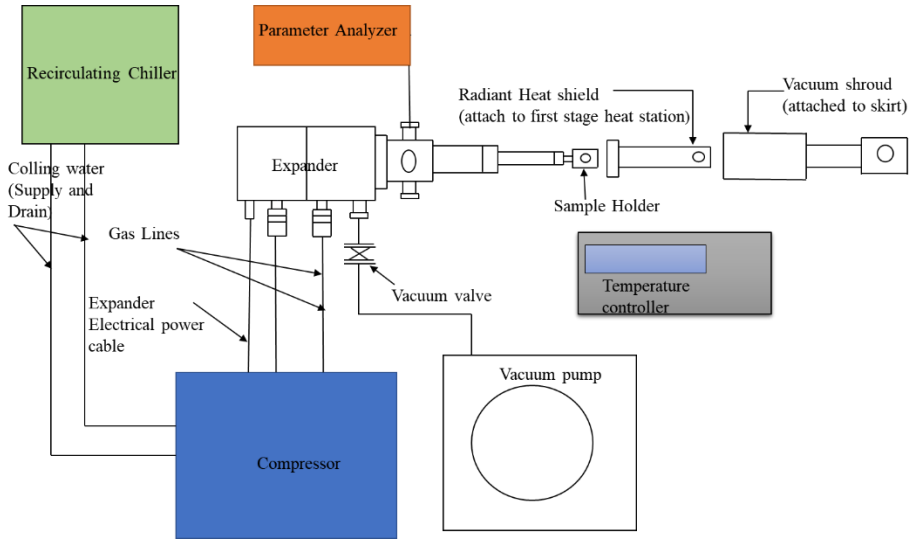

Figure 3.1 Schematic diagram of closed cycle cryostat setup.

3.1.1 Cryocooler

The cryocooler has two main components, the cold head and compressor; this is the heart of the system. Here we used DE 202 cryocooler which is light in weight and available for a wide range of temperature from 4^{o} K to 450^{o} K. This cryocooler has designed for low sample vibration so we can avoid noise. Figure 3.2 shows Cold head with sample holder that has two stage heat station.

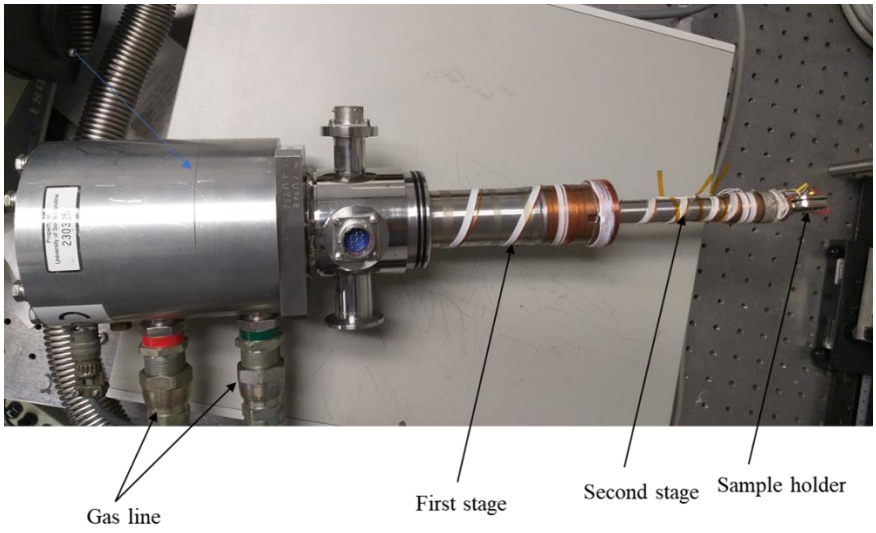

Figure 3.2 Cold head with the sample holder.

3.1.2 Vacuum shroud

The vacuum shroud is made from stainless steel or aluminum. Stainless steel is more suitable to use for vacuum shroud as it is more durable and less susceptible to adsorbing water vapor making which make cleaner sample environment. Aluminum is cost-effective and available in a wide variety of configurations. Figure 3.3 represents the vacuum shroud. A typical vacuum shroud will be mounted on the cryocooler using double O-rings for vacuum seal. This allows us to rotate the vacuum shroud without losing the vacuum.

Figure 3.3 Vacuum shroud of the cryostat.

3.1.3 Radiation Shield

The radiation shield is made from copper or aluminum. Figure 3.4 represents vacuum shroud. High purity copper is high durability and low emissivity. Copper radiation shield with nickel or gold, gives the surface low thermal emissivity for better performance. Nickel plating is more durable than gold.

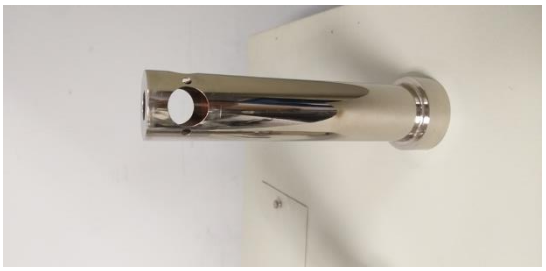

Figure 3.4 Radiation shield of the cryostat.

3.1.4 Sample Holder

Sample holder constructed from copper or nickel plat which has high thermal conductivity. Sample holders have electrical pins for an easy connection for the device do electrical and optical study of the samples. Sample holders have designed such way so we can easily connect LEDs Device.

3.1.5 Optical windows

Optical window material can be made from Quartz, Sapphire, CsI, KBr, ZnSe. We select optical windows in such a way to avoid absorption of UV light so we can get light outside of the optical window to analyze. The wavelength of optical window material can be visible or UV light. The thickness of the window depends on its diameter and the material. Thin windows are advisable for collecting weak optical signals. The large and thicker window are used for high vacuum forces.

3.1.6 Temperature control

The temperature control system has a sensor and a heater to achieve the desired temperature. The temperature controller has dual channels; one is for sample temperature monitoring and the other for control. Temperature controller heater used to stabilize temperature by feedback from the sensor during the experiments. Accuracy of reading the sample temperature depends on where we mounted the temperature sensor. To minimize the experimental error, we can locate the sensor close to the sample so that we can get the actual temperature. We use a temperature controller to monitor the temperature and control temperature of the cryocooler from room temperature to 8K.

3.1.7 Vacuum pump

The vacuum pump is used for creating a good vacuum. Having a good vacuum in the cryostat is mandatory for many reasons. The better the vacuum, the lower the device temperature. The absolute temperature and conductive cooling are linear function low pressure. Most importantly, the vacuum prevents the water condensation on the sample and helps attain low temperature.

3.1.8 Compressor

The Compressor is one of the most essential components for cryostat set up. Compressors provide high-pressure helium gas to the cryocooler. The compressor also connects with recirculating chiller, which provides cooling water to the compressor. Here we use Advance system research, ARS-4HW compressor for our research. ARS-4HW required 230 V supply voltage. ARS-4HW required low maintenance so it is convenient for research purposes.

3.2 Semiconductor parameter analyzer

We use Agilent 4156B semiconductor parameter analyzer. This analyzer used for the measurement of LEDs. The 4156B allows us two types of measurements, sampling measurement and the sweep measurement. It also provides knob sweep measurement. The 4156 B have two voltage measurement unit and two voltage source unit. It has a kelvin connection, so it is highly suitable for low resistance applications. Voltage range for Agilent 4156B is 0 to 100V and current range is 1pA to 100mA. We used the 4156B to apply voltage to our LEDs and measure the V-I characteristic of LEDs. We can save data for the V-I characteristic using a floppy disk. We also used the 4156B to apply a 20mA Dc pump current and measure the EL characteristic of LEDs.

3.3 Spectrometer

Ocean optics USB 2000 spectrometer was used for measuring the electroluminescence properties of DUV LEDs. Here the spectrometer relates to window Xp via USB port. The spectrometer gets power from the host computer. The USB 2000 can control by Ocean view software OOIBASE32. USB 2000 has good responsivity and very high sensitivity. It has integration time from 1 milli second to 60 seconds. USB 2000 has EEPROM storage for wavelength calibration coefficients and Linearity correction coefficients. The wavelength range for USB 2000 Ocean optics spectrometer is 200nm - 1100 nm. We need to store reference and dark measurement for to correct instrument response and variables. Figure 3.5 represents a schematic diagram of the spectrometer. The light from the light LED collect to detector and pass-through optical fiber. Optical fiber transmits light to spectrometer USB 2000. The USB 2000 spectrometer measure amount of light and transforms the collected data by the spectrometer into digital

information. The spectrometer transmits data to spectrometer operating software OOIBASE 32. The OOIBASE 32 compares the sample data to reference measurement and displays spectral information on the computer screen. We can save data in the the computer. For low-temperature measurement, we can save data for different temperature and compare data with different temperatures.

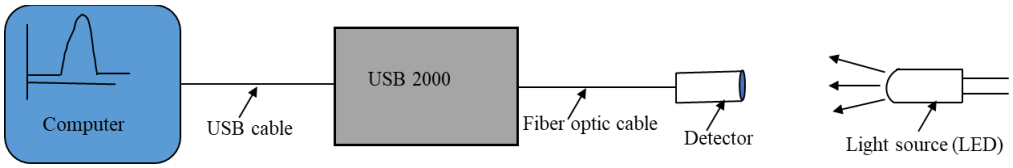

Figure 3.5 Schematic diagram of the spectrometer.

3.4 Device testing conditions and consideration

To measure LEDs at low temperatures, we need to care about testing, and it is required some conditions are mentioned below.

(1) To measure LED at low temperature, we need to package LED so connect LED to sample holder. The size of the package should be no more than 1.81 inches or 46 millimeters, which is the diameter of the radiation shield.

(2) Wire bonding is required to measure LED at low temperatures. We cannot measure LED in cryocooler without packaging, and package devices require wire bonding for electrical connection. For the high current applications, we required ball to wedge bonding. Ball formation is required on gold pads of LEDs, so the current spread on the ball to apply high current.

(3) To get an accurate result of electroluminescence (EL) and V-I characteristic of LED at different temperatures we need to wait for 5 minutes to stabilize temperature then measure.

(4) To measure electroluminescence (EL) at low temperature, it is required dark atmosphere.

(5) To measure LED at low temperature, we need to close the cryostat perfectly to creates a vacuum inside the cryocooler.

(6) To measure LED at low temperature, first we need to turn on the vacuum pump and wait until the pressure is below 20m Torr, switch on the chiller then turn on the compressor.

CHAPTER 4

RESULTS AND DISCUSSION

In chapter 2, we briefly discuss structure of DUV LED and the packaging of DUV LEDs. In chapter 3 discuss the experimental procedure for LEDs which includes an overview of the cryostat, parameter analyzer and spectrometer. This chapter describe the temperature dependent electroluminescence (EL) and Temperature dependent I-V characteristic.

4.1 Temperature dependent electroluminescence (EL)

This section focuses on temperature dependent study of EL spectra of DUV LEDs. Figure 4.1 represents El spectra of Micro DUV LEDs at applied 20 mA DC pump current in the temperature range from 10K to 300K using close- cycle He cryostat. Details about the experiment set up for this measurement discussed in chapter 3. The El was measured in the temperature range from 10 K to 300K using Agilent 4156B semiconductor parameter analyzer. Figure 4.1 represents that as temperature decrease band to band emission increased. The MQW emission intensity grow rapidly with a drop in temperature, as all defects freeze out at very low temperature, so El emission reach its maximum at 10K. The MQW's band-to–band emission peak intensity increases at low temperature by more than four-fold. Note that an increase in intensity is a function of the DC pump current. We can say that light emitted efficiency increases with a decrease in temperature due to the non-radiative carrier rate is decrease and radiative recombination rate is increased. DUV LEDs have high Al-content $Al_xGa_{1-x}N$ allow are suitable to the

formation of threading dislocation, defect like dislocation but we see that at low temperature it starts to freeze out.

However, Zang J illustrate low temperature electroluminescence quenching of AlGaN DUV-LEDs [61]. In this paper they study three different AlGaN DUV LED, in which two LED do not have Electron blocking layer (EBL) and one have EBL where they observed EL quenching in AlGaN DUV LEDs which do not have EBL. We can expect that the electron overflow become more severe as temperature decrease if you do not have EBL. X. A. Cao et al get a similar result for temperature dependent study of InGaN/GaN multiple-quantum-well light emitting diode, they found that El intensity increases rapidly with decease in temperature and reaches its maximum at 150 K, as temperature decrease 150 K a remarkable reduction noticed in light intensity. We also observed similar results for our conventional DUV LED. Figure 4.2 represent temperature dependent EL spectra of DUV micro-LED at the injection current of 20mA (DC pump). We observed that El intensity increases with a decrease in the temperature and reached its maximum at 110 K; as temperature decrease below110 K, a remarkable reduction in light intensity is seen.

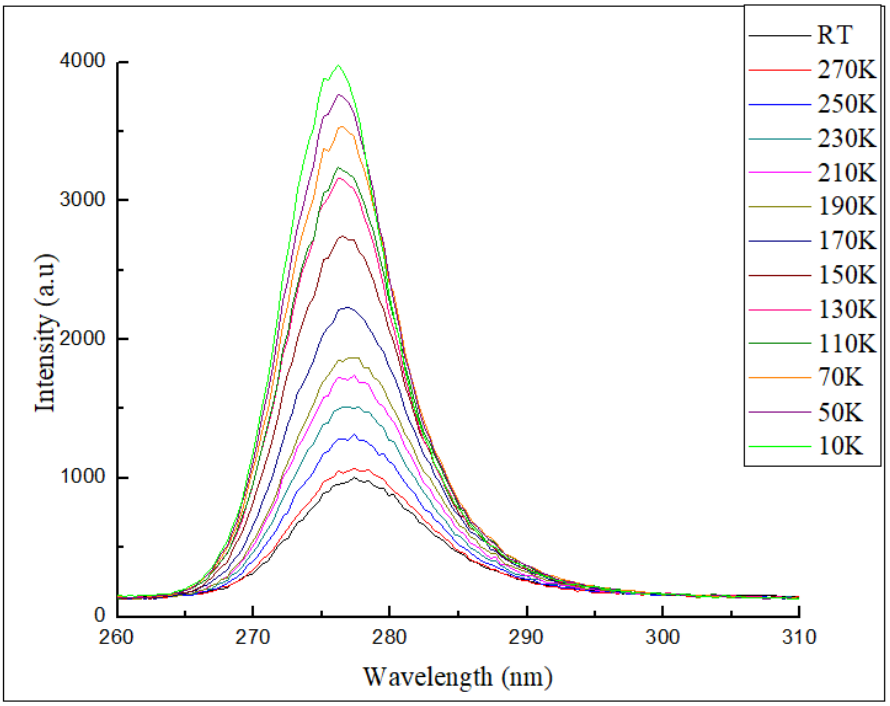

Figure 4.1 Temperature dependent EL spectra of DUV micro-LED at the injection current of 20mA (DC pump).

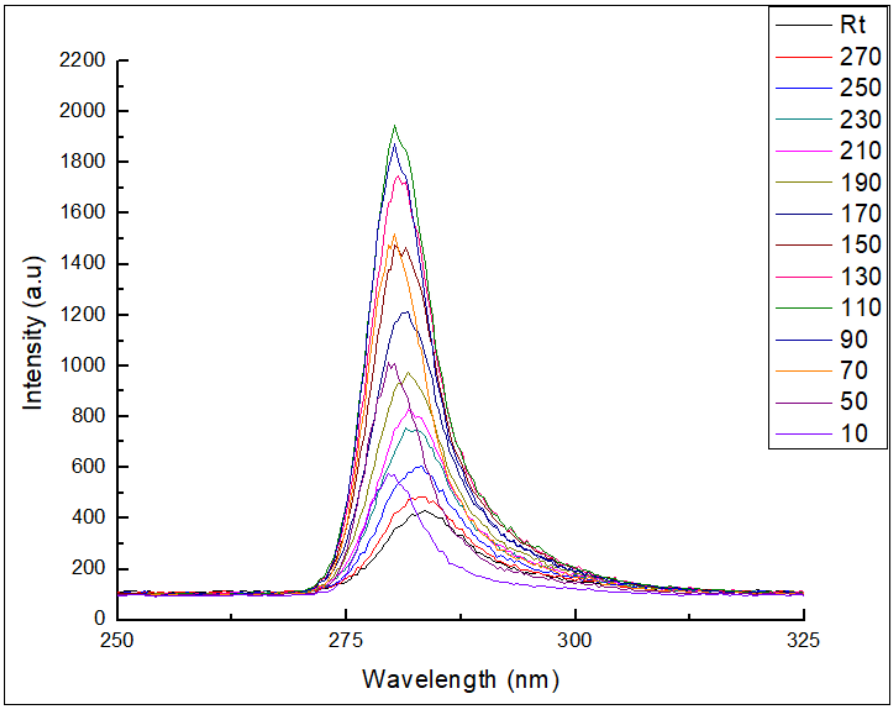

Figure 4.2 Temperature dependent EL spectra of conventional DUV LED at the injection current of 20mA (DC pump).

Figure 4.3(a) presents peak intensity of MQW band to band emission peak located at 280nm increase fast with reduction of temperature from 300K to 10K. We observed low intensity at room temperature (300K) and high intensity at 10K. The peak intensity increases at low temperature by a factor of four, suggesting that light emitted efficiency increases with a decrease in temperature due to the non-radiative rate is decrease at low temperature in micro DUV-LED. We have high light emitted efficiency at 10K and low light emitted efficiency at room temperature (300 K). However, in our conventional DUV LED peak EL intensity increases with decease in the temperature and peaked at 110 K, as temperature decrease below110 K a remarkable reduction noticed in EL peak light intensity is observed that is shown in figure 4.3(b).

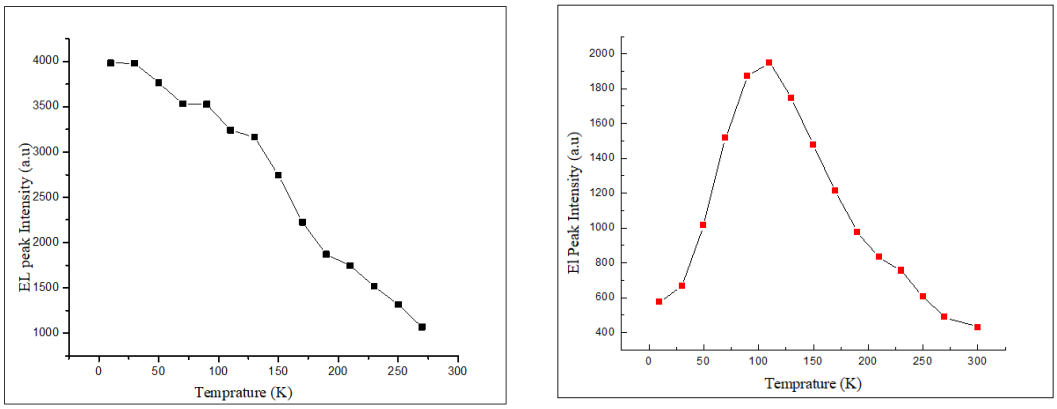

(a) (b)

Figure 4.3 (a) El peak intensity change with temperature for (a) DUV micro-LED (b) conventional DUV-LED.

Figure 4.4 present temprature- induced shift of peak energy of LEDs at applied 20 mA DC pump current in temperature range from 10K to 300K. With decreasing temperature, we see blueshift behavior for both Micro LED and conventional LED. As temperature decrease peak potion of photon energy move toward shorter wavelength so we see blueshift. As temperature decrease bandgap of LED is increase means energy

increase which means wavelength is decrease because wavelength is inversely proposal to energy (E= $\frac{1.24}{\lambda\,(\mu m)}$).

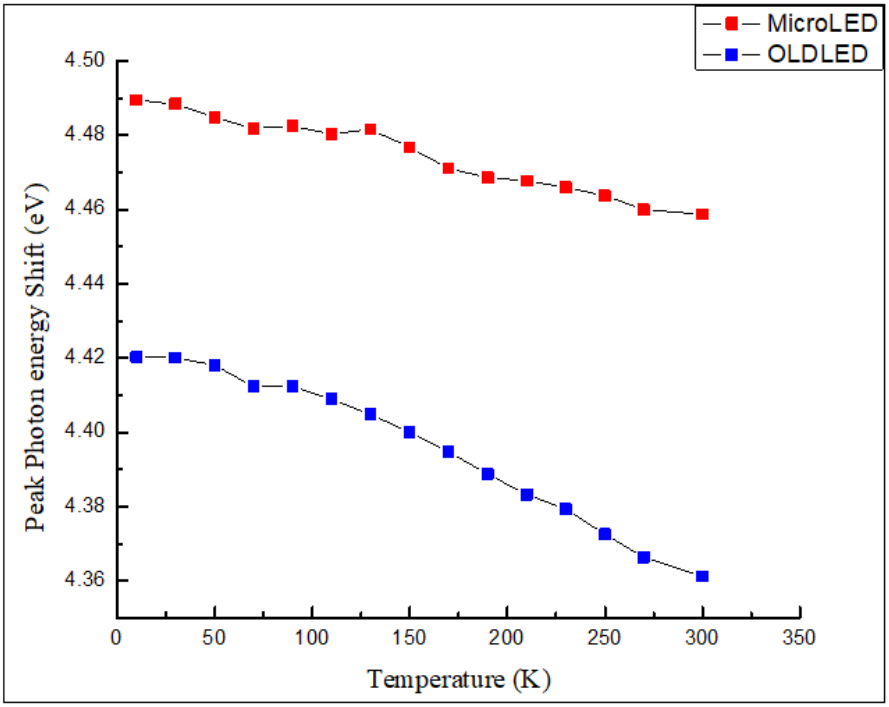

Figure 4.4 EL peak energy shift of micro-LED and conventional DUV-LED at applied 20 mA DC pump current.

The IQE is the product of the injection efficiency (IE) and the radiative efficiency (RE) where the RE is defines as the ratio of the radiative recombination rate to total recombination and the IE is a measure of how many electrons recombine in active region to total electrons injected into an LED. Here we assumed that IE is 100% so we can simply study IQE. Figure 5.5 present temperature dependent IQE, as temperature decrease, IQE is increase because non radiative recombination lifetimes is decrease.

$\eta_{IQE} = \eta_{IE}\ x\eta_{RE}$

Where,

IE is the injection efficiency and RE is the radiative efficiency.

$$\eta_{RE} = \frac{1}{1+\frac{\tau r}{\tau nr}}$$

where,

τr is the lifetime for radiative recombination and τnr is the lifetime for non-radiative recombination.

At low temperature (10K), the non-radiative recombination rate is low which means non radiative recombination lifetime is high because non-radiative recombination rate is inversely proportional to lifetime of recombination (R= $\Delta n/\tau nr$). We get high IQE at low temperature compared to room temperature.

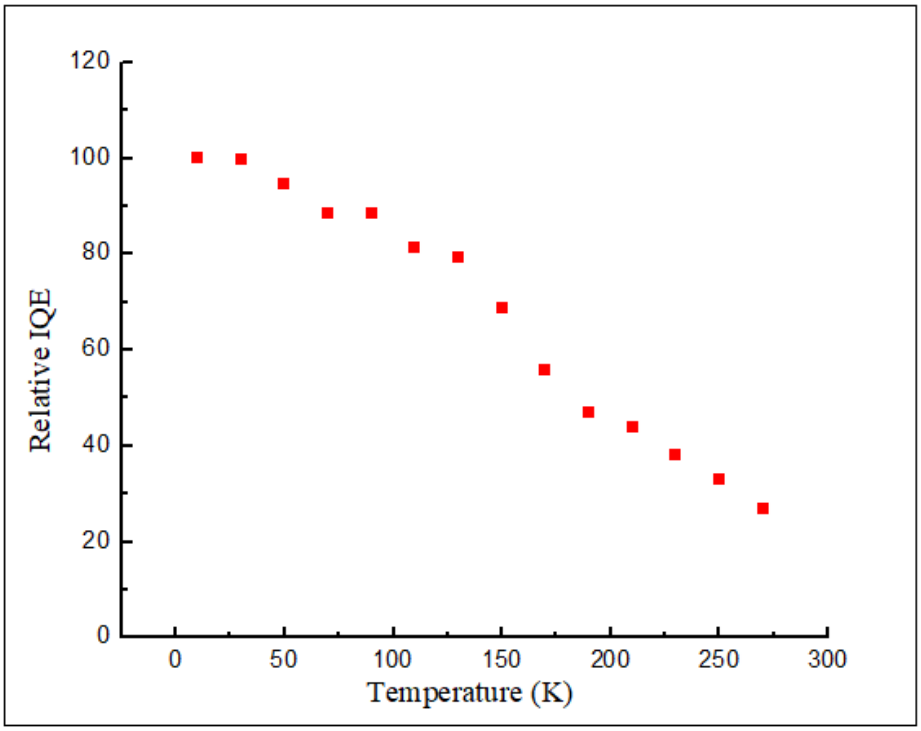

Figure 4.5 Temperature dependent relative internal quantum efficiency (IQE).

4.2 Temperature dependent current-voltage (V-I) Characteristic.

This section focuses on temperature dependent study of the V-I characteristic of Micro DUV- LED. We plotted the current versus voltage (I-V) characteristic of the Micro

DUV LED in the temperature range of 10-300 K using an Agilent 4156B semiconductor parameter analyzer. We are not able to measure accurately current smaller than 10^{-14} A because of system limitation.

Figure 4.6 present a model for micro DUV-LED; we proposed a more accurate circuit model to combine with Sandia national laboratory and Schubert group work[73], [74]. Sandia national laboratory presents the V-I characteristics of AlGaN based DUV-LED with different densities of open-core threading dislocation (nano pipes). Open core threading dislocations create a low turn-on leakage pathway which we have seen in our V-I characteristic of micro DUV-LED. Schubert group presented a model for diode ideality factor greater than 2.0, as per Sah-Noyce-Shockley theory, the forward current in p-n junction is dominated by recombination of minority carrier injected into the natural region of the junction, this type of current give ideality factor 1.0. Recombination of the carriers in the space charge region give us an ideality factor 2.0. Schubert group proposed ideality factor greater than 2.0 because of diode connected in series, so ideality factor add together. The metal-semiconductor contact which can consider as a reverse-biased Schottky contact have high ideality factor. They connect Multiple diodes in series for a heterojunction III-N DUV LED structure at the p-GaN/p-AlGaN interface. So, we proposed our model to combine both models.

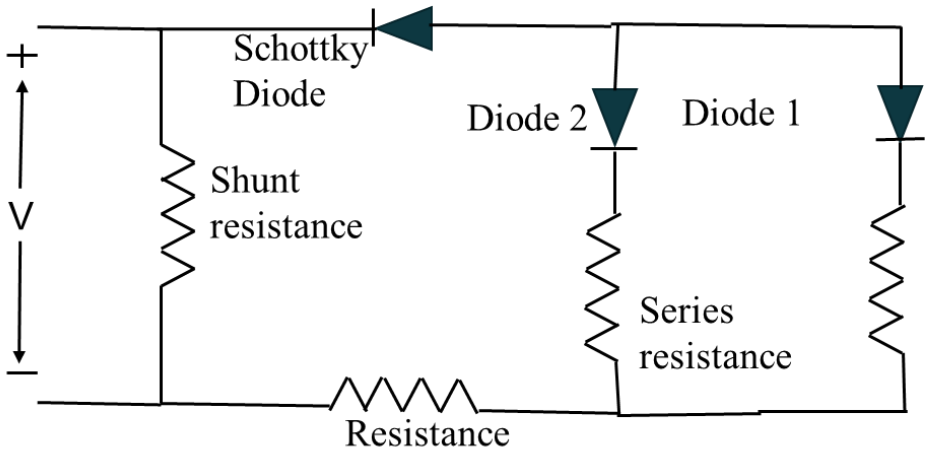

Figure 4.6 Equivalent circuit model of V-I characteristic of micro DUV- LED.

The forward current versus voltage (I-V) characteristic of the Micro DUV LED in the temperature range of 10-300 K in figure 4.7 (a). The I-V curve of Micro DUV LED is plotted on the semilogarithmic scale in figure 4.7(b). For 0V to 2V shunt resistance dictates I-V curve, voltage is not sufficient to turn on leakage diode nor induce tunneling at the Schottky diode. For 2.7V to 4.2 V, diode 1 (leakage diode) is turn-on and leakage diode path has less resistance than shunt resistance so current flows through leakage diode. For 4.2 to 5.5 V, carrier begins through diode 2 start to conduct, this means more voltage can drop over MQW diode, and when this voltage become higher than built-in, the MQW diode begins to conduct. Carriers are recombined in the MQW region, and light generation starts at this time leakage diode (diode 1) is still conducting which provides an alternative current path that reduces the number of carriers flowing through the MQW-diode path. For voltage ≥ 5.5 V, carriers are tunneling through the Schottky barrier diode; all the other diodes are well into their conductive region of operation thus the series resistance of the LED dictates the shape of the I-V plot. Michael W et al. found similar results for AlGaN based DUV LED; they made three diode circuit models to explain forward IV characteristics [73].

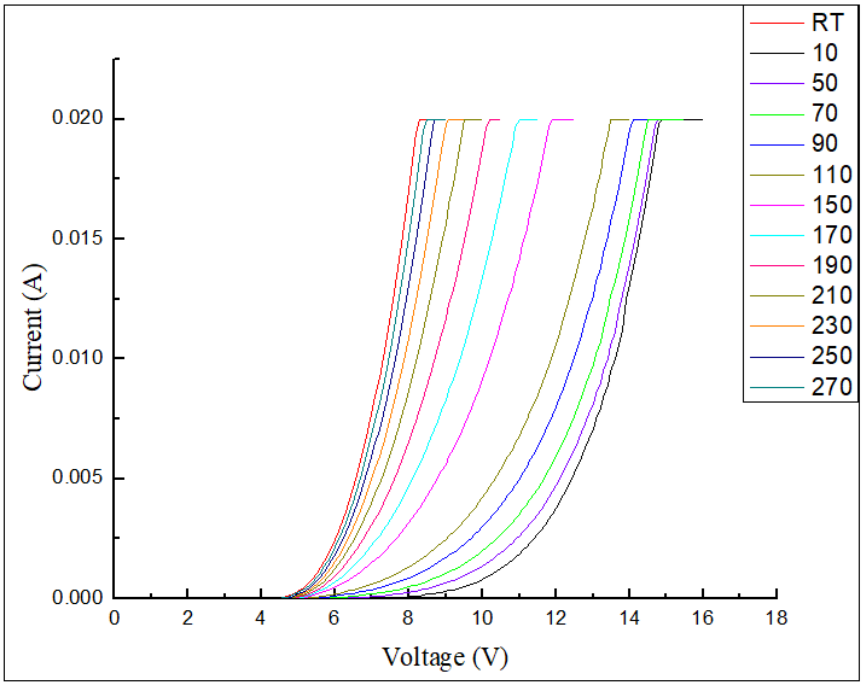

(a)

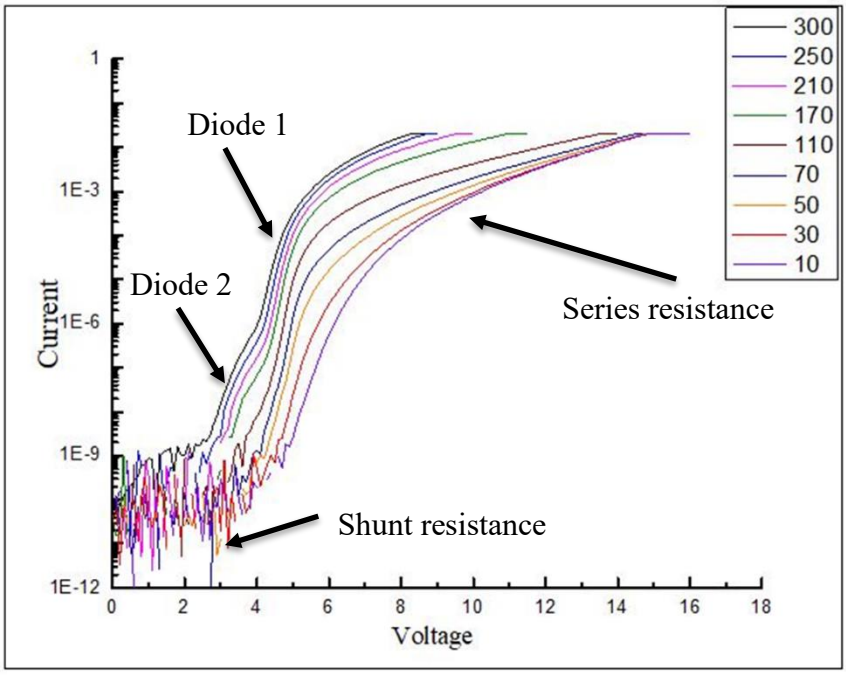

(b)

Figure 4.7 (a) Forward-bias IV characteristic of micro DUV LED. (b) IV characteristic of Micro DUV LED are plotted on a semilogarithmic scale for different temperature.

The forward bias V-I characteristic of micro DUV -LEDs were model in MATLAB using two parallel diodes. In MATLAB, we are very the current and calculate voltage drop across the junction. The reverse diode in series represent Schottky diode. Parameter for diode and resistor of circuit extracted from the DUB -LED V-I characteristic from Figure 4.8 (a), which represent measured and simulated characteristic of DUV LED at 300K and Figure 4.8 (b) present measured and simulated characteristic of DUV LED at 190K.

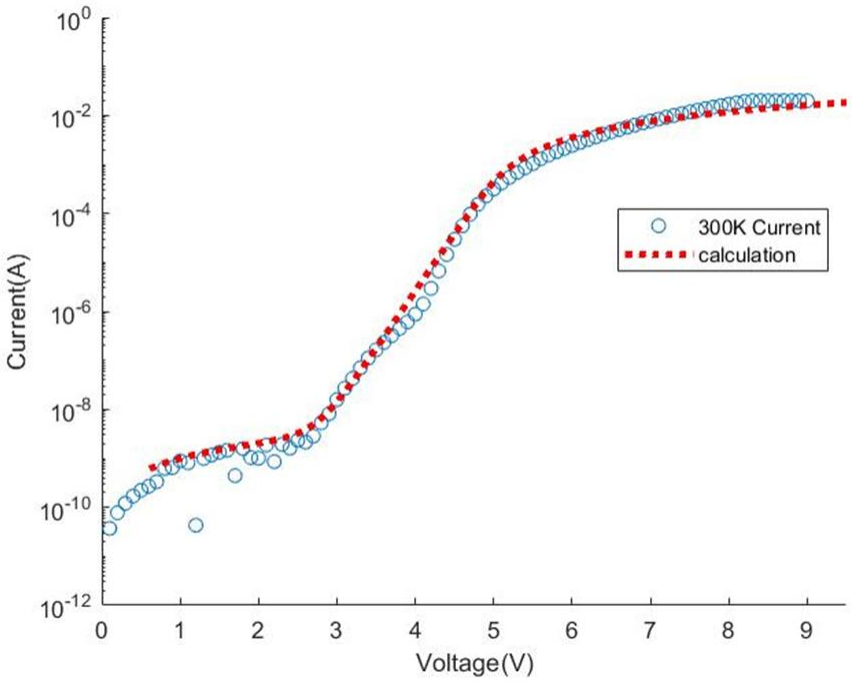

(a)

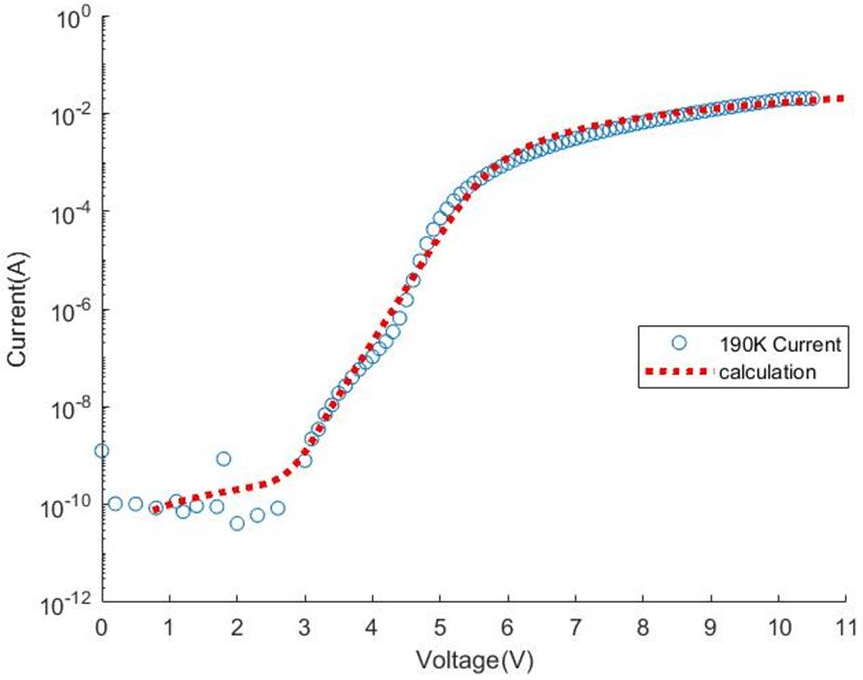

(b)

Figure 4.8 (a) Measure and simulated V-I characteristic of micro DUV- LED at 300K. (b) measure and simulated V-I characteristic of micro-DUV LED for 190K.

A thorough analysis of the I-V characteristics shows a low turn-on pathway with (2.7) eV barrier that we ascribe to field emission through threading dislocations or surface recombination at device edge; and a higher turn-on pathway of (4.3 eV) that shows thermionic field emission behavior, ascribed to the MQW-based P-N junction. We also analyzed that, we can see a low turn-on pathway until 50K, after that defect start to freeze out, and the low turn-on voltage path disappears. Figure 4.9 represent V-I characteristic of micro DUV-LED at three different temperature, we see that leakage path disappear at low temperature which means, whatever is causing the leakage can freeze-out at low temperatures. Perhaps it was a clustering of the dopants on the walls of the open-core threading dislocations (nano pipes) that caused this leakage.

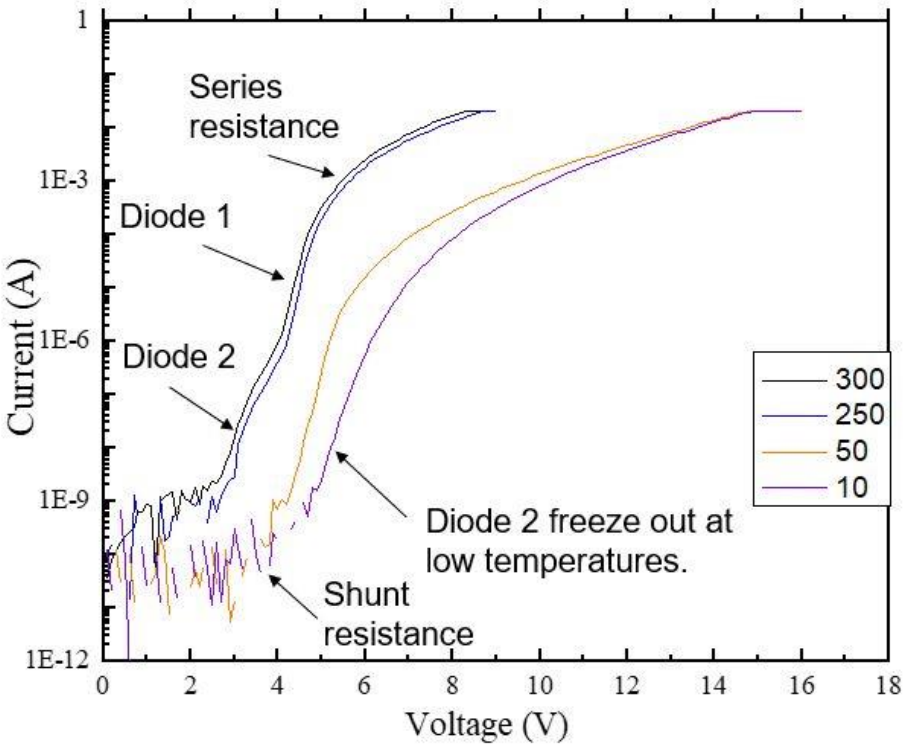

Figure 4.9 V-I characteristic of micro DUV-LED at three different temperature.

The ideality factor of a diode is defined as how closely the diode follows ideal the diode equation. The ideality factor of the diode is determined from the slope of the forward bias current (ln(I)) versus voltage plot. The ideality factor of two regions, leakage diode and MQW diode where current increase exponentially is defined as

$$n = \frac{q}{kT}\left(\frac{dV}{dI}\right)$$

where V is forward-bias voltage, I is current, k is the Boltzmann constant, T is absolute temperature and q is the change of an electron.

Figures 4.10 (a) and 4.10 (b) represent temperature dependent ideality factor for leak diode and MQW diode. For voltage < 4 V, we can find ideality factor for leakage diode and for voltage > 4 V, ideality factor for MQW diode. Figure 4.10 (a) and (b),

show that the ideality factor of both diodes increases with reduced temperature. We find ideality factor 5.21 at room temperature for the MQW diode. But, as per Sah-Noyce-Shockley theory, the forward current in p-n junction is dominated by recombination of minority carrier injected into the natural region of the junction, this type of current give ideality factor 1.0. Recombination of carriers in the space charge region gives us ideality factor 2.0[74]. However, we find a high ideality factor for micro-DUV LED because of the MWQ region and metal-semiconductor junction of the LED. High value of ideality factor is attributed to the carrier tunneling rather than to the thermal diffusion and recombination (as described by Shubert et al.). The carrier tunneling in space charge region because of high doping of the active layer or due to high density of localized state. Figure 4.10 (a) and (b), we see that the ideality factor increases with reduction in temperature. Recombination through threading dislocation pathway, we find ideality factor 9.8 at room temperature and find ideality factor 28 at 100 k. For MQW based p-n junction, we see ideality factor 5.21 at room temperature and find ideality factor 204.98 at 10K. The high ideality factor that gets worse with temperature is due to the worsening of metallic contacts and their interface with the semiconductor, ideality factor is already high at 300K for this diode.

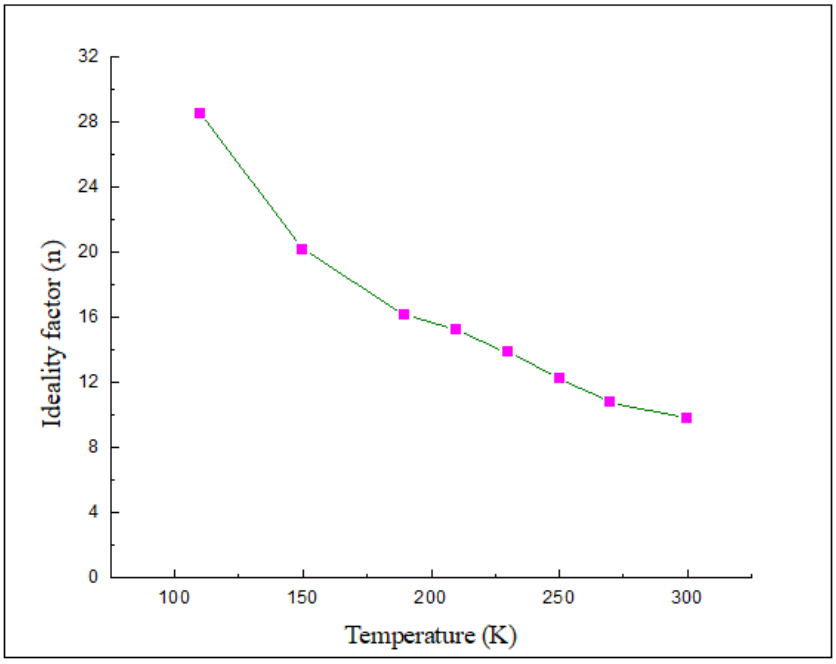

(a)

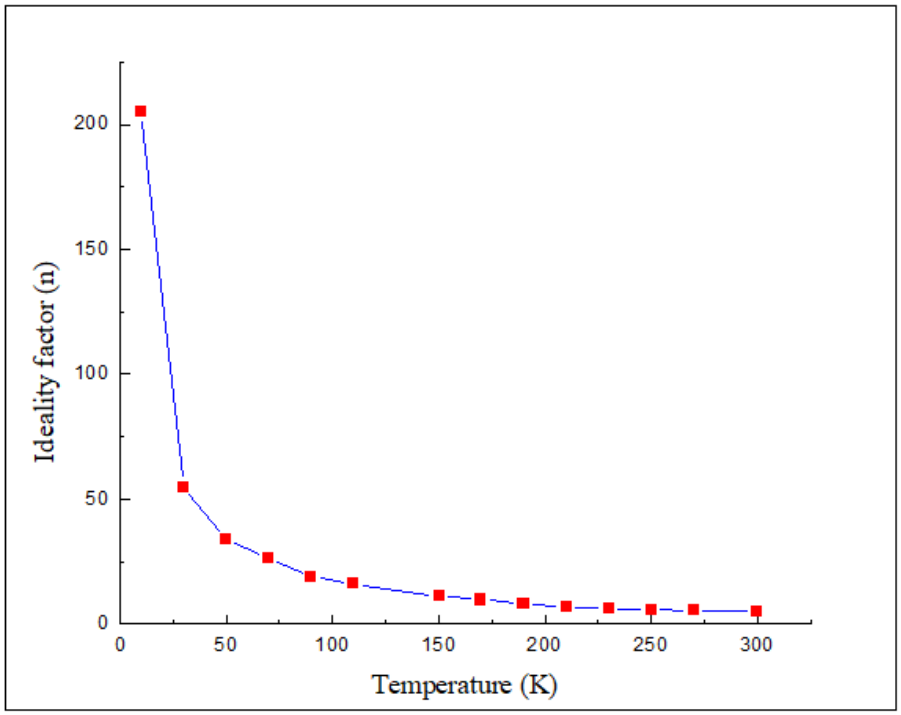

(b)

Figure 4.10 Temperature dependent ideality factor (a) for leakage diode (diode 1) and (b) for MQW diode (diode 2).

We can get the turn-on voltage of LED from the x-axis intercept from a linear fit to the linear region of the I-V graph. Figure 4.11 represents the change in turn-on voltage of micro-DUV LED change with temperature. LED turn-on voltage increase from 6.39 at room temperature to 12.37 at 10K. The turn-on voltage of about 6.39 V at 300K is somewhat larger than expected from an active layer band gap of 4.5eV, showing an additional voltage drop at the heterointerfaces and voltage drop at metal semiconductor interface. The increase of turn-on voltage is much larger than expected from the active layer band gap change with temperature and reverse Schottky diode. This is reflected in the increased turn-on voltage with decreasing temperature

The device series resistance was measured in temperature range from 300 K to 10K. Figure 4.12 (a) represents the linear region for series resistance extraction, and Figure 4.12 (b) represents series resistance change with temperature. From room temperature (300K) to 150 K, series resistance increases with reductions in temperature but from 150K to 10K, series resistance decreases with reduction in temperature. The resistance changes from 94Ω at 300K to 124 Ω at 10K. The variation in resistance with temperature are primarily due to hole accumulation at AlGaN/GaN interface and p-GaN layer thickness. The increase of resistance is related to electron hopping transport along with the impurity state in highly doped n layers.

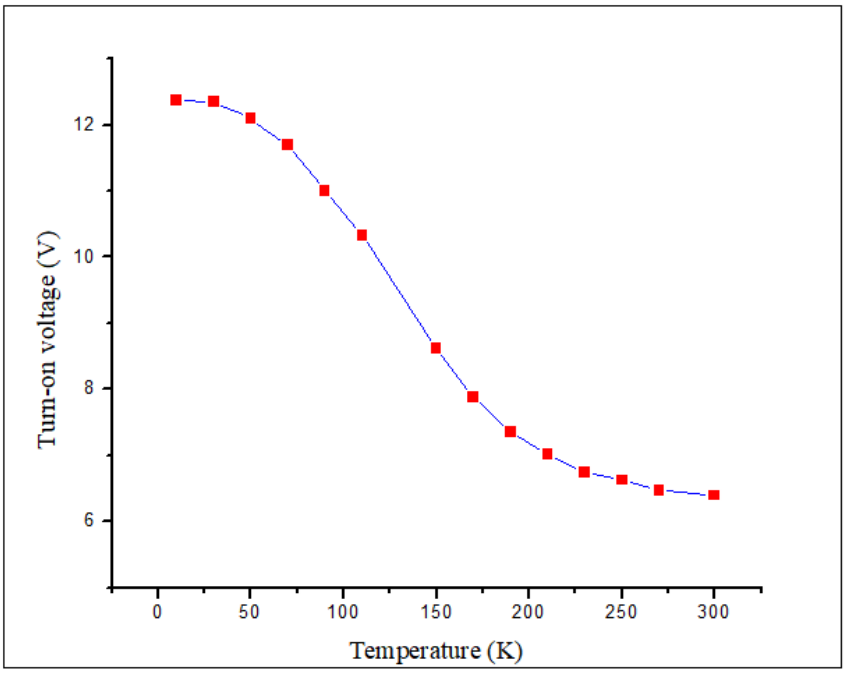

Figure 4.11 Micro-DUV LED turn-on voltage change with temperature.

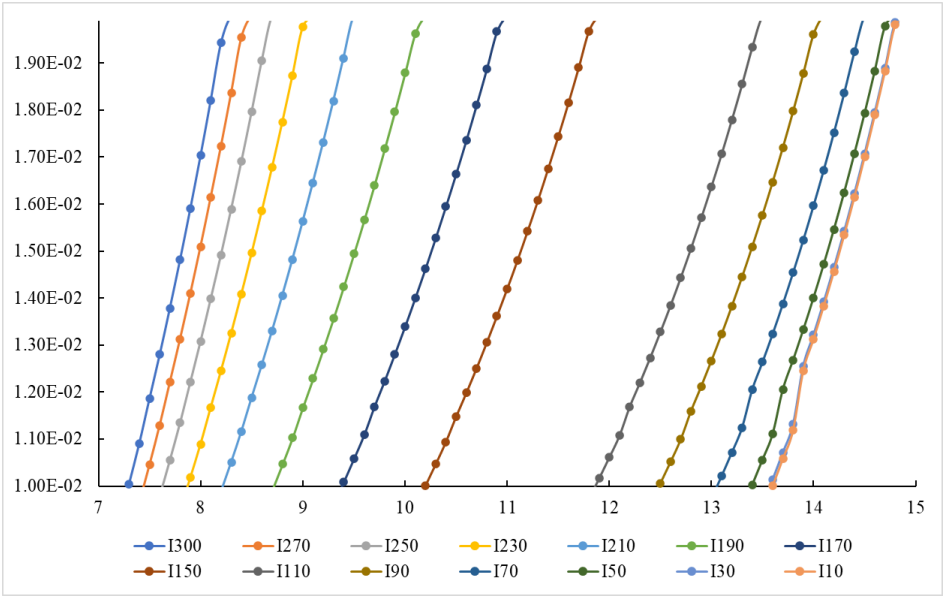

(a)

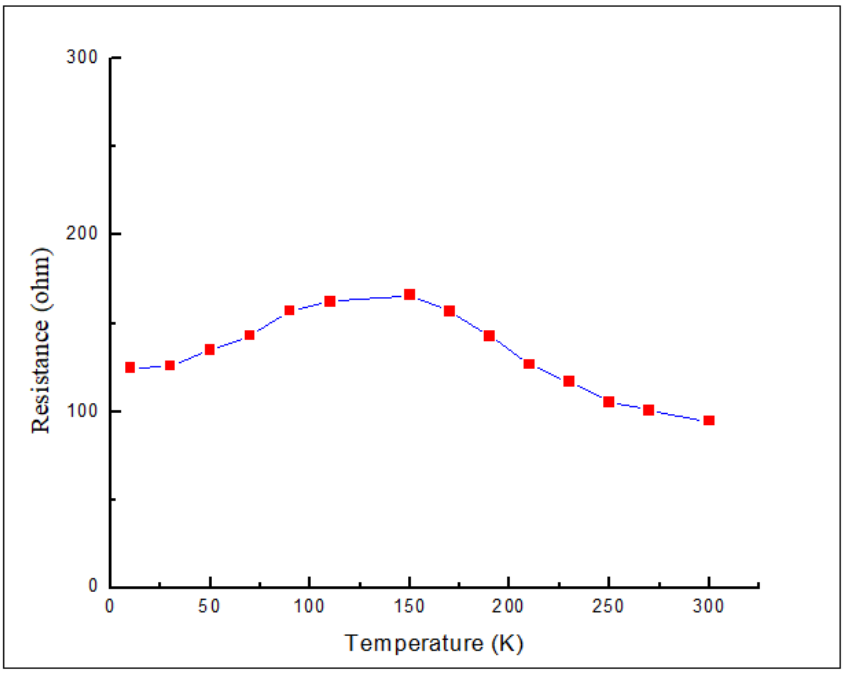

(b)

Figure 4.12 (a) Linear region for series resistance extraction. (b) Series resistances change with temperature.

CHAPTER 5

CONCLUSIONS AND FUTURE WORK

In this dissertation, the temperature dependent behavior of the Micro-pixeled DUV-LEDs has been studied we briefly discuss structure of DUV LED and packaging of DUV LEDs. We also describe the temperature dependent electroluminescence (EL) and Temperature dependent I-V characteristics. We observed defect-related conduction pathways at temperatures greater than 70K. The forward bias V-I characteristic of micro DUV -LEDs were model in MATLAB using two parallel diode and one series diode. By freezing out defect related conduction pathways at temperatures less than 50K, the EQE in AlGaN DUV micro-LEDs is improved 4-fold, underscoring the importance of defect management. A thorough analysis of the I-V characteristics shows a low turn-on pathway with (2.7) eV barrier that we ascribe to field emission through threading dislocations or surface recombination; and a higher turn-on pathway of (4.3) eV that shows thermionic field emission behavior, ascribed to the MQW-based P-N junction. The parasitic conduction paths are caused by open-core threading dislocations, as informed by thorough reports in the literature.

Hence, targeted improvement of strain management techniques during growth to reduce the open-core threading dislocation density is of great importance for furthering the EQE of DUV micro-emitters.

REFERENCES

[1] D. Zhu, D. J. Wallis, and C. J. Humphreys, “Prospects of III-nitride optoelectronics grown on Si,” *Reports on Progress in Physics*, vol. 76, no. 10, Oct. 2013, doi: 10.1088/0034-4885/76/10/106501.

[2] E. Fred. Schubert, *Light-emitting diodes*. Cambridge University Press, 2006.

[3] S. C. Jain, M. Willander, J. Narayan, and R. van Overstraeten, “APPLIED PHYSICS REVIEWS III-nitrides: Growth, characterization, and properties,” 2000. [Online]. Available: http://ojps.aip.org/japo/japcr.jsp.

[4] T. Mukai, M. Yamada, and S. Nakamura, “cite this article: Shuji Nakamura et al,” 1995.

[5] T. Mukai, M. Yamada, and S. Nakamura, “Current and Temperature Dependences of Electroluminescence of InGaN-Based UV/Blue/Green Light-Emitting Diodes,” Publication Board, 1998.

[6] T. Mukai, M. Yamada, and S. Nakamura, “Related content InGaN-based violet laser diodes S Nakamura-Current and Temperature Dependences of Electroluminescence of InGaN-Based UV/Blue/Green Light-Emitting Diodes Characteristics of InGaN-Based UV/Blue/Green/Amber/Red Light-Emitting Diodes,” Publication Board, 1999.

[7] J. Han *et al.*, “AlGaN/GaN quantum well ultraviolet light emitting diodes,” *Applied Physics Letters*, vol. 73, no. 12, pp. 1688–1690, 1998, doi: 10.1063/1.122246.

[8] T. Nishida, H. Saito, and N. Kobayashi, “Efficient and high-power AlGaN-based ultraviolet light-emitting diode grown on bulk GaN,” *Applied Physics Letters*, vol. 79, no. 6, pp. 711–712, Aug. 2001, doi: 10.1063/1.1390485.

[9] H. Hirayama, Y. Enomoto, A. Kinoshita, A. Hirata, and Y. Aoyagi, “Efficient 230-280 nm emission from high-Al-content AlGaN-based multiquantum wells,” *Applied Physics Letters*, vol. 80, no. 1, pp. 37–39, Jan. 2002, doi: 10.1063/1.1432112.

[10] W. H. Sun *et al.*, “AlGaN-based 280 nm light-emitting diodes with continuous wave powers in excess of 1.5 mW,” *Applied Physics Letters*, vol. 85, no. 4, pp. 531–533, Jul. 2004, doi: 10.1063/1.1772864.

[11] V. Adivarahan *et al.*, “250 nm AlGaN light-emitting diodes,” *Applied Physics Letters*, vol. 85, no. 12, pp. 2175–2177, Sep. 2004, doi: 10.1063/1.1796525.

[12] V. Adivarahan *et al.*, “High-efficiency 269 nm emission deep ultraviolet light-emitting diodes,” *Applied Physics Letters*, vol. 84, no. 23, pp. 4762–4764, Jun. 2004, doi: 10.1063/1.1756202.

[13] I. Gherasoiu *et al.*, “Growth mechanism of AIN by metal-organic molecular beam epitaxy,” *Journal of Applied Physics*, vol. 96, no. 11, pp. 6272–6276, Dec. 2004, doi: 10.1063/1.1813623.

[14] L. Tian, N. Stojanovic, D. Y. Song, A. A. Bernussi, J. M. Berg, and M. Holtz, “Influence of photonic nanotexture on the light extraction efficiency of GaN,” *Applied Physics Letters*, vol. 91, no. 10, 2007, doi: 10.1063/1.2783474.

[15] S. X. Jin, J. Li, J. Y. Lin, and H. X. Jiang, “InGaN/GaN quantum well interconnected microdisk light emitting diodes,” *Applied Physics Letters*, vol. 77, no. 20, pp. 3236–3238, Nov. 2000, doi: 10.1063/1.1326479.

[16] Y. Taniyasu, M. Kasu, and T. Makimoto, “An aluminium nitride light-emitting diode with a wavelength of 210 nanometres,” *Nature*, vol. 441, no. 7091, pp. 325–328, May 2006, doi: 10.1038/nature04760.

[17] H. Hirayama, T. Yatabe, N. Noguchi, T. Ohashi, and N. Kamata, “231-261 nm AlGaN deep-ultraviolet light-emitting diodes fabricated on AlN multilayer buffers grown by ammonia pulse-flow method on sapphire,” *Applied Physics Letters*, vol. 91, no. 7, 2007, doi: 10.1063/1.2770662.

[18] H. Hirayama, “Quaternary InAlGaN-based high-efficiency ultraviolet light-emitting diodes,” *Journal of Applied Physics*, vol. 97, no. 9. May 01, 2005, doi: 10.1063/1.1899760.

[19] S. Fujikawa, T. Takano, Y. Kondo, and H. Hirayama, “Realization of 340-nm-band high-output-power (>7mW) InAlGaN quantum well ultraviolet light-emitting diode with p-type InAlGaN,” *Japanese Journal of Applied Physics*, vol. 47, no. 4 PART 2, pp. 2941–2944, Apr. 2008, doi: 10.1143/JJAP.47.2941.

[20] M. Kneissl *et al.*, “Ultraviolet semiconductor laser diodes on bulk AlN,” *Journal of Applied Physics*, vol. 101, no. 12, 2007, doi: 10.1063/1.2747546.

[21] M. H. Kim *et al.*, “Origin of efficiency droop in GaN-based light-emitting diodes,” *Applied Physics Letters*, vol. 91, no. 18, 2007, doi: 10.1063/1.2800290.

[22] J. H. Park *et al.*, “Enhanced overall efficiency of GaInN-based light-emitting diodes with reduced efficiency droop by Al-composition-graded AlGaN/GaN superlattice electron blocking layer,” *Applied Physics Letters*, vol. 103, no. 6, Aug. 2013, doi: 10.1063/1.4817800.

[23] Y. Zhang *et al.*, “Light extraction efficiency improvement by multiple laser stealth dicing in InGaN-based blue light-emitting diodes,” *Optics Express*, vol. 20, no. 6, p. 6808, Mar. 2012, doi: 10.1364/oe.20.006808.

[24] P. Dong *et al.*, “282-nm AlGaN-based deep ultraviolet light-emitting diodes with improved performance on nano-patterned sapphire substrates,” *Applied Physics Letters*, vol. 102, no. 24, Jun. 2013, doi: 10.1063/1.4812237.

[25] M. Kneissl, T. Y. Seong, J. Han, and H. Amano, “The emergence and prospects of deep-ultraviolet light-emitting diode technologies,” *Nature Photonics*, vol. 13, no. 4. Nature Publishing Group, pp. 233–244, Apr. 01, 2019, doi: 10.1038/s41566-019-0359-9.

[26] Y. Narukawa, M. Ichikawa, D. Sanga, M. Sano, and T. Mukai, “White light emitting diodes with super-high luminous efficacy,” *Journal of Physics D: Applied Physics*, vol. 43, no. 35, Sep. 2010, doi: 10.1088/0022-3727/43/35/354002.

[27] M. Lachab *et al.*, “Optically-pumped 285 nm edge stimulated emission from AlGaN-based LED structures grown by MOCVD on sapphire substrates,” *Japanese Journal of Applied Physics*, vol. 53, no. 11, Nov. 2014, doi: 10.7567/JJAP.53.112101.

[28] R. Jain *et al.*, “Migration enhanced lateral epitaxial overgrowth of AlN and AlGaN for high reliability deep ultraviolet light emitting diodes,” *Applied Physics Letters*, vol. 93, no. 5, 2008, doi: 10.1063/1.2969402.

[29] I. Ahmad *et al.*, “Dislocation reduction in high Al-content AlGaN films for deep ultraviolet light emitting diodes,” *Physica Status Solidi (A) Applications and Materials Science*, vol. 208, no. 7, pp. 1501–1503, Jul. 2011, doi: 10.1002/pssa.201001104.

[30] H. Hirayama, T. Yatabe, T. Ohashi, and N. Kamata, “Remarkable enhancement of 254-280 nm deep ultraviolet emission from AlGaN quantum wells by using high-quality AlN buffer on sapphire,” in *Physica Status Solidi (C) Current Topics in Solid State Physics*, 2008, vol. 5, no. 6, pp. 2283–2285, doi: 10.1002/pssc.200778697.

[31] A. Chitnis *et al.*, “High-quality p-n junctions with quaternary AlInGaN/InGaN quantum wells,” *Applied Physics Letters*, vol. 77, no. 23, pp. 3800–3802, Dec. 2000, doi: 10.1063/1.1331084.

[32] T. Kolbe *et al.*, “Effect of electron blocking layer doping and composition on the performance of 310 nm light emitting diodes,” *Materials*, vol. 10, no. 12, Dec. 2017, doi: 10.3390/ma10121396.

[33] M. R. Kwon, T. H. Park, T. H. Lee, B. R. Lee, and T. G. Kim, “Improving the performance of AlGaN-based deep-ultraviolet light-emitting diodes using electron blocking layer with a heart-shaped graded Al composition,” *Superlattices and Microstructures*, vol. 116, pp. 215–220, Apr. 2018, doi: 10.1016/j.spmi.2018.02.033.

[34] H. Hirayama, Y. Tsukada, T. Maeda, and N. Kamata, “Marked enhancement in the efficiency of deep-ultraviolet AlGaN light-emitting diodes by using a multiquantum-barrier electron blocking layer,” *Applied Physics Express*, vol. 3, no. 3, Mar. 2010, doi: 10.1143/APEX.3.031002.

[35] S. Fujikawa, H. Hirayama, and N. Maeda, “High-efficiency AlGaN deep-UV LEDs fabricated on a- and m-axis oriented c-plane sapphire substrates,” *Physica Status Solidi (C) Current Topics in Solid State Physics*, vol. 9, no. 3–4, pp. 790–793, Mar. 2012, doi: 10.1002/pssc.201100453.

[36] H. Hirayama, N. Maeda, S. Fujikawa, S. Toyoda, and N. Kamata, “Recent progress and future prospects of AlGaN-based high-efficiency deep-ultraviolet light-emitting diodes,” *Japanese Journal of Applied Physics*, vol. 53, no. 10, Oct. 2014, doi: 10.7567/JJAP.53.100209.

[37] S. I. Inoue, N. Tamari, and M. Taniguchi, “150 mW deep-ultraviolet light-emitting diodes with large-area AlN nanophotonic light-extraction structure emitting at 265 nm,” *Applied Physics Letters*, vol. 110, no. 14, Apr. 2017, doi: 10.1063/1.4978855.

[38] J. Yun and H. Hirayama, “Investigation of the light-extraction efficiency in 280 nm AlGaN-based light-emitting diodes having a highly transparent p-AlGaN layer,” *Journal of Applied Physics*, vol. 121, no. 1, Jan. 2017, doi: 10.1063/1.4973493.

[39] S. I. Inoue, T. Naoki, T. Kinoshita, T. Obata, and H. Yanagi, “Light extraction enhancement of 265 nm deep-ultraviolet light-emitting diodes with over 90 mW output power via an AlN hybrid nanostructure,” *Applied Physics Letters*, vol. 106, no. 13, Mar. 2015, doi: 10.1063/1.4915255.

[40] C. E. Lee *et al.*, “Luminance enhancement of flip-chip light-emitting diodes by geometric sapphire shaping structure,” *IEEE Photonics Technology Letters*, vol. 20, no. 3, pp. 184–186, Feb. 2008, doi: 10.1109/LPT.2007.912990.

[41] M. Shatalov *et al.*, “Large chip high power deep ultraviolet light-emitting diodes,” *Applied Physics Express*, vol. 3, no. 6, Jun. 2010, doi: 10.1143/APEX.3.062101.

[42] J. Mickevičius, G. Tamulaitis, M. Shur, M. Shatalov, J. Yang, and R. Gaska, “Correlation between carrier localization and efficiency droop in AlGaN epilayers,” *Applied Physics Letters*, vol. 103, no. 1, Jul. 2013, doi: 10.1063/1.4813259.

[43] M. Shatalov *et al.*, “AlGaN deep-ultraviolet light-emitting diodes with external quantum efficiency above 10%,” *Applied Physics Express*, vol. 5, no. 8, Aug. 2012, doi: 10.1143/APEX.5.082101.

[44] J. R. Grandusky *et al.*, “270nm pseudomorphic ultraviolet light-emitting diodes with over 60mW continuous wave output power,” *Applied Physics Express*, vol. 6, no. 3, Mar. 2013, doi: 10.7567/APEX.6.032101.

[45] J. R. Grandusky, S. R. Gibb, M. C. Mendrick, C. Moe, M. Wraback, and L. J. Schowalter, “High output power from 260nm pseudomorphic ultraviolet light-emitting diodes with improved thermal performance,” *Applied Physics Express*, vol. 4, no. 8, Aug. 2011, doi: 10.1143/APEX.4.082101.

[46] T. Kinoshita *et al.*, “Performance and reliability of deep-ultraviolet light-emitting diodes fabricated on AlN substrates prepared by hydride vapor phase epitaxy,” *Applied Physics Express*, vol. 6, no. 9, Sep. 2013, doi: 10.7567/APEX.6.092103.

[47] C. Pernot *et al.*, “Improved efficiency of 255-280 nm AlGaN-based light-emitting diodes,” *Applied Physics Express*, vol. 3, no. 6, Jun. 2010, doi: 10.1143/APEX.3.061004.

[48] A. Fujioka, T. Misaki, T. Murayama, Y. Narukawa, and T. Mukai, “Improvement in output power of 280-nm deep ultraviolet light-emitting diode by using AIGaN multi quantum wells,” *Applied Physics Express*, vol. 3, no. 4, Apr. 2010, doi: 10.1143/APEX.3.041001.

[49] K. Ding, V. Avrutin, Ü. Özgür, and H. Morkoç, “Status of growth of group III-nitride heterostructures for deep ultraviolet light-emitting diodes,” *Crystals*, vol. 7, no. 10. MDPI AG, Oct. 01, 2017, doi: 10.3390/cryst7100300.

[50] J. Y. Shin, S. J. Kim, D. K. Kim, and D. H. Kang, “Fundamental characteristics of deep-UV light-emitting diodes and their application to control foodborne pathogens,” *Applied and Environmental Microbiology*, vol. 82, no. 1, pp. 2–10, 2016, doi: 10.1128/AEM.01186-15.

[51] H. Hirayama, N. Maeda, S. Fujikawa, S. Toyoda, and N. Kamata, “Recent progress and future prospects of AlGaN-based high-efficiency deep-ultraviolet light-emitting diodes,” *Japanese Journal of Applied Physics*, vol. 53, no. 10, Oct. 2014, doi: 10.7567/JJAP.53.100209.

[52] H. Hirayama, “Recent Progress in AlGaN Deep-UV LEDs,” in *Light-Emitting Diode - An Outlook On the Empirical Features and Its Recent Technological Advancements*, InTech, 2018.

[53] “Topics in Applied Physics.” [Online]. Available: www.springer.com/series/560.

[54] H. M. El-Hennawy, “Code: E 10 COMPARISON STUDY OF HBT DEVICES BASED-ON ALGAAS/GAAS AND ALGAN/GAN,” 2014. [Online]. Available: https://www.researchgate.net/publication/281742067.

[55] W. Sun *et al.*, “Continuous wave milliwatt power AlGaN light emitting diodes at 280 nm,” *Japanese Journal of Applied Physics, Part 2: Letters*, vol. 43, no. 11 A, Nov. 2004, doi: 10.1143/JJAP.43.L1419.

[56] A. Chitnis *et al.*, “Improved performance of 325-nm emission AlGaN ultraviolet light-emitting diodes,” *Applied Physics Letters*, vol. 82, no. 16, pp. 2565–2567, Apr. 2003, doi: 10.1063/1.1569040.

[57] M. Kneissl, T. Y. Seong, J. Han, and H. Amano, “The emergence and prospects of deep-ultraviolet light-emitting diode technologies,” *Nature Photonics*, vol. 13, no. 4. Nature Publishing Group, pp. 233–244, Apr. 01, 2019, doi: 10.1038/s41566-019-0359-9.

[58] A. Chitnis *et al.*, “Self-heating effects at high pump currents in deep ultraviolet light-emitting diodes at 324 nm,” *Applied Physics Letters*, vol. 81, no. 18, pp. 3491–3493, Oct. 2002, doi: 10.1063/1.1518155.

[59] G. D. Hao, M. Taniguchi, N. Tamari, and S. I. Inoue, “Current crowding and self-heating effects in AlGaN-based flip-chip deep-ultraviolet light-emitting diodes,” *Journal of Physics D: Applied Physics*, vol. 51, no. 3, Jan. 2018, doi: 10.1088/1361-6463/aa9e0e.

[60] R. Floyd *et al.*, “An opto-thermal study of high brightness 280 nm emission AlGaN micropixel light-emitting diode arrays,” *Applied Physics Express*, vol. 14, no. 1, p. 014002, Jan. 2021, doi: 10.35848/1882-0786/abd140.

[61] J. C. Zhang, Y. Sakai, and T. Egawa, “Low-temperature electroluminescence quenching of AlGaN deep ultraviolet light-emitting diodes,” *Applied Physics Letters*, vol. 96, no. 1, 2010, doi: 10.1063/1.3284521.

[62] A. Chitnis *et al.*, “Low-temperature operation of AlGaN single-quantum-well light-emitting diodes with deep ultraviolet emission at 285 nm,” *Applied Physics Letters*, vol. 81, no. 16, pp. 2938–2940, Oct. 2002, doi: 10.1063/1.1516631.

[63] A. Chitnis *et al.*, “Milliwatt Operation of Sapphire Based 340 nm UV LEDs with Quaternary AlInGaN Quantum Wells at Room and Cryogenic Temperatures,” 2001.

[64] J. I. Shim, D. P. Han, C. H. Oh, H. Jung, and D. S. Shin, “Measuring the internal quantum efficiency of light-emitting diodes at an arbitrary temperature,” *IEEE Journal of Quantum Electronics*, vol. 54, no. 2, Apr. 2018, doi: 10.1109/JQE.2018.2795044.

[65] A. G. Thompson, “= __-_ @ Materials Update MOCVD technology for semiconductors,” 1997.

[66] J. Zhang *et al.*, “AlGaN deep-ultraviolet light-emitting diodes,” *Japanese Journal of Applied Physics, Part 1: Regular Papers and Short Notes and Review Papers*, vol. 44, no. 10, pp. 7250–7253, Oct. 2005, doi: 10.1143/JJAP.44.7250.

[67] P. Capper, S. Irvine, and T. Joyce, “Epitaxial crystal growth: methods and materials,” in *Springer Handbooks*, Springer, 2017, p. 1.

[68] Z. Cheng *et al.*, “Experimental observation of high intrinsic thermal conductivity of AlN,” *Physical Review Materials*, vol. 4, no. 4, Apr. 2020, doi: 10.1103/PhysRevMaterials.4.044602.

[69] Y. R. Koh *et al.*, “Bulk-like Intrinsic Phonon Thermal Conductivity of Micrometer-Thick AlN Films,” *ACS Applied Materials and Interfaces*, vol. 12, no. 26, pp. 29443–29450, Jul. 2020, doi: 10.1021/acsami.0c03978.

[70] V. Adivarahan *et al.*, “280nm deep ultraviolet light emitting diode lamp with an algan multiple quantum well active region,” *Applied Physics Express*, vol. 2, no. 10, Oct. 2009, doi: 10.1143/APEX.2.102101.

[71] J. P. Zhang *et al.*, “Algan multiple-quantum-well-based, deep ultraviolet light-emitting diodes with significantly reduced long-wave emission,” *Applied Physics Letters*, vol. 83, no. 17, pp. 3456–3458, Oct. 2003, doi: 10.1063/1.1623321.

[72] M. Shatalov *et al.*, “Thermal analysis of flip-chip packaged 280 nm nitride-based deep ultraviolet light-emitting diodes,” *Applied Physics Letters*, vol. 86, no. 20, pp. 1–3, May 2005, doi: 10.1063/1.1927695.

[73] M. W. Moseley, A. A. Allerman, M. H. Crawford, J. J. Wierer, M. L. Smith, and A. M. Armstrong, “Detection and modeling of leakage current in AlGaN-based deep ultraviolet light-emitting diodes,” *Journal of Applied Physics*, vol. 117, no. 9, Mar. 2015, doi: 10.1063/1.4908543.

[74] J. M. Shah, Y. L. Li, T. Gessmann, and E. F. Schubert, “Experimental analysis and theoretical model for anomalously high ideality factors (n≫2.0) in AlGaN/GaN p-n junction diodes,” *Journal of Applied Physics*, vol. 94, no. 4, pp. 2627–2630, Aug. 2003, doi: 10.1063/1.1593218.